T-2203

MODIFIED BIPOLE-DIPOLE SURVEY, BELL CREEK OIL FIELD

by

Nancy Jo House

ProQuest LLC.
789 East Eisenhower Parkway
P.O. Box 1346
Ann Arbor, MI 48106 – 1346

T-2203

A thesis submitted to the Faculty and Board of Trustees of the Colorado School of Mines in partial fulfillment of the requirements for the degree of Master of Science in Geophysics.

Golden, Colorado

Date 4 May ,1979

Signed: Nancy Jo House
Nancy Jo House
Student

Approved: George V. Keller
George V. Keller
Thesis Advisor

Golden, Colorado

Date 4 May , 1979

George V. Keller
George V. Keller
Head of Department

ABSTRACT

In July of 1978 a modified bipole-dipole survey was conducted over the Bell Creek oil field, in southeastern Montana to determine the feasibility of directly detecting oil by means of direct current measurements made on the surface.

Four dipole potential difference measurements were made at 42 stations from each of two sources. Potential differences were converted to total electrical field and apparent resistivities calculated. Second vertical derivatives were then calculated from the four total electric fields at each observation point. Finally, the potential differences were converted to monopole potentials and these inverted to causative dipole moments/unit area on an imaginary grid at the approximate depth of the oil field.

Results of analysis indicate that the oil is detectable on the surface. Positive dipole moments appeared over the thickest portion of the pay zone as a result of inversion of the potential. Positive values of the second vertical derivatives of the potential field also appear to have significant correlation to thick portions of the producing formation.

TABLE OF CONTENTS

3 pg 7 6's

LIST OF FIGURES

ACKNOWLEDGEMENTS

I would to express my gratitude to Dr. George Keller for suggesting this project and acting as my thesis advisor, Dr. Alexander Kauffman, for serving on my committee, and Dr. Charles Stoyer for serving on my committee and helping with computer programming.

Brandon Brygider, Pat James, and Sue O'Connell helped a great deal in the drafting of many of the figures.

I would also like to give special thanks to Mary Jane House for spending many long hours typing the manuscript.

The field work for this project was funded by the Integrated Geophysics Project. My work on the project was supported by an HEW Fellowship.

INTRODUCTION

Exploration for oil has been achieved historically through indirect methods. These included geologic studies of structure and stratigraphy through surface mapping techniques and extrapolation of available subsurface geologic data subsequent to exploration drilling. More recently the seismic reflection method has had considerable success at locating structures which might contain hydrocarbons and within the last ten years the presence of high amplitude reflections have been associated with gas accumulations.

Use of electrical methods for oil exploration has been discussed and at times attempted since the early 1920's. Discussions in the geophysical literature from the early 1930's until the present, point toward the potential usefulness of electrical methods for mapping of subsurface geologic structure, location of lithologic changes leading to oil entrapment and the direct detection of oil accumulations from surface measurements.

The physical property of a rock which is most significantly affected by the presence of oil in the pore spaces is its electrical conductivity. This effect can be expressed by examining Archie's Law:

$$\rho = \rho_w S_w^{-n} \varphi^{-m}$$

Where: ρ is the bulk resistivity of the sample,

ρ_w is the resistivity of the fluid in the pore spaces,

S_w is the porosity expressed as a fraction/unit volume,

φ is the fraction of pore spaces filled with fluid,

and m and n are empirical constants which are determined experimentally to make the measurements fit a particular set of data.

The equations used for describing the behavior of the field in direct current methods are particularly simple. These are: the divergence of the current density,

$$\nabla \cdot \mathbf{J} = 0$$

the relationship between the electric field and the scalar potential,

$$\mathbf{E} = -\nabla U$$

and Ohm's Law.

$$\mathbf{E} = \rho \mathbf{J}$$

These give rise to Poisson's equation,

$$\nabla^2 U = -\rho \nabla U \cdot \nabla (1/\rho)$$

Which reduces to Laplace's equation,

$$\nabla^2 U = 0$$

When: 1) ρ is constant

2) ρ is zero

or 3) the potential is constant $\nabla U = 0$

When there is a contrast in resistivity between two layers the first condition for Laplace's equation to hold will be violated within that region of space, and a surface charge will arise on that surface. This surface charge density will create a secondary field according to Coulomb's Law which will enhance or detract from the primary field according to its polarity. Solutions for the value of the secondary field have been calculated previously in the literature. (e.g. Keller, 1968)

The parameter which most influences direct current measurements made on the surface is the transverse resistance of the media. The transverse resistance of a given layer in a horizontally layered earth is the resistance which a $1m^2$ column of that rock would present to current flowing through it vertically. This would be expressed as:

$$T_i = \rho_i h_i$$

Where: T_i is the transverse resistance of the i^{th} layer of the medium,

ρ_i is the resistivity of the i^{th} layer,

and h_i is the thickness of the i^{th} layer.

The transverse resistance of the entire geoelectric section consisting of m layers would be written as:

$$T_i = \sum_{i=1}^{m} T_i = \sum_{i=1}^{m} \rho_i h_i$$

Transverse resistance contrast, as used here, is the ratio of the transverse resistance of the oil bearing zone divided by the total transverse resistance of the medium overlying it (T_2/T_1). The anomaly in the resistivity as measured from the surface is a function of the ratio of dipole receiver length to the depth of the thin resistant layer. The maximum anomaly will be observed from a thin layer having a transverse resistance contrast of 1 per cent with a spacing between source and receiver electrodes of about three times the depth to the oil bearing zone. The anomaly in resistivity in this case would be near one per cent.

In the summer of 1978 a bipole-dipole survey was conducted over the Belle Creek Oil Field in southeastern Montana, in an attempt to determine whether or not it would be possible to delineate changes in direct current electrical phenomena due to the presence of oil.

The Bell Creek oil field has been interpreted geologically as a barrier island in the northern portion and a delta in the southwestern portion (McGreogor and Biggs, 1968). The producing formation, the Muddy Sandstone, is between 3 and 15 meters thick (10 and 50 feet) and lies at a depth of 1.3 kilometers (4300 feet) in the survey area. It is immediatley overlain by a few hundred meters of Mowry shale and underlain by a few hundred meters of Skull creek shale.

Well logs were obtained for the oil field and the area surrounding it, figure 1. The portion of the geologic section above the pay zone was divided into four geoelectric units. Well logs were digitized and an average resistivity for each of the four units determined. The resistivity of each unit was plotted for each well in its appropriate location. These values were then contoured. Maps of the succesive units from the surface to the unit above the Muddy Sandstone are shown in figures 1-a,2,2, and 4.

Each unit exhibits relatively high resistivities within the survey area. The top unit (1) has an average resistivity of between 14 and 20 ohm-meters, compared to between 8 and 10 ohm-meters in the surrounding area. Unit 2 has a fairly constant resistivity of 3-3.5 ohm-meters within the area shown. The resistivity of unit 3 is 7 ohm-meters within the survey area and decreases gradually to 4 ohm-meters on the northern edge of the area covered by

well logs. The resistivity of unit 4 was between 5 and 6 ohm-meters within the survey area and decreases to 3.5 ohm-meters towards the edge of the map prepared for this study. Although the geoelectric section above the Muddy Sandstone exhibits higher resistivities within the survey area than the surrounding area, the resistivities of all of the units were fairly constant within this region.

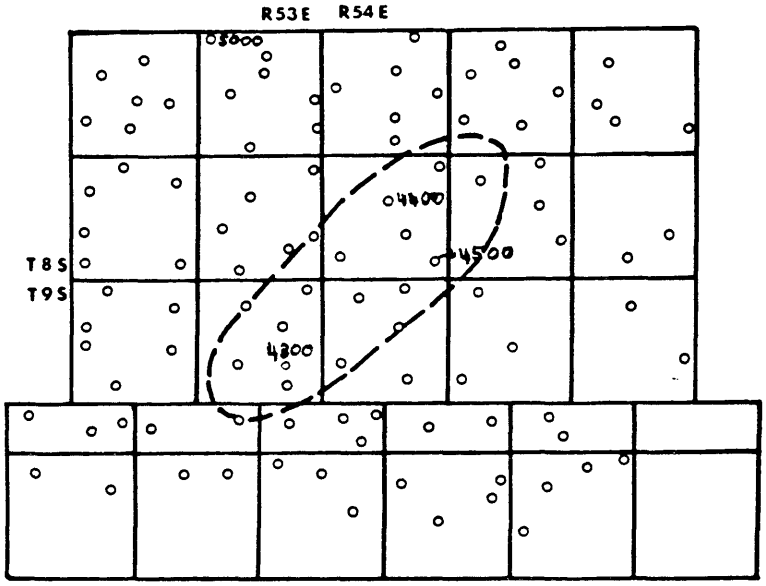

Figure 1. Location of wells selected for average resistivity determinations of geo-electric units. Depth to top of Muddy Sand-stone shown for selected wells.

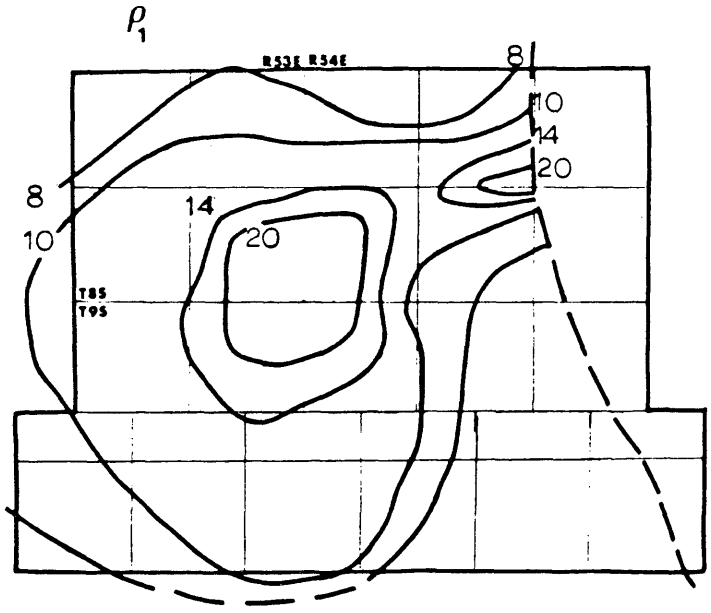

Figure 1-a. Average resistivity of geo-electric unit 1 from well log analysis.

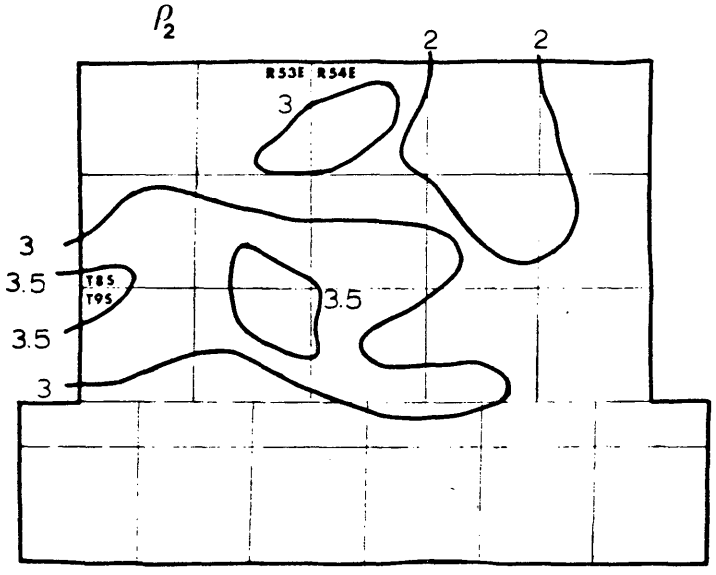

Figure 2. Average resistivity of geo-electric unit 2 form well log analysis.

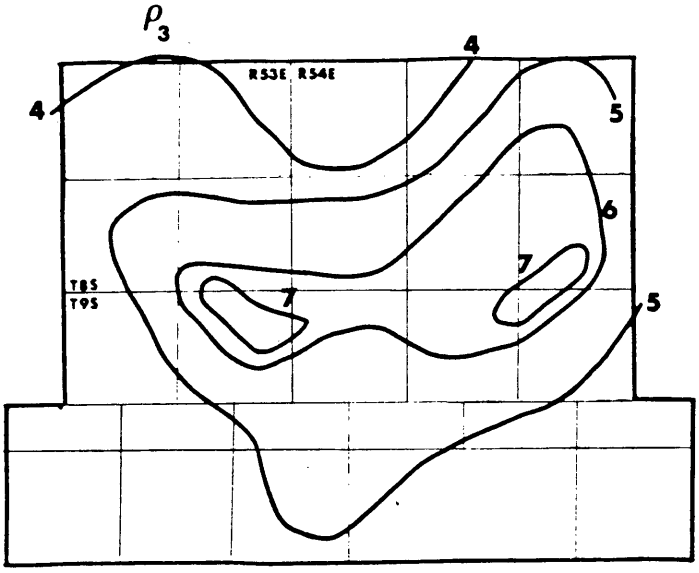

Figure 3. Average resistivity of geoelectric unit 3 from well log analysis

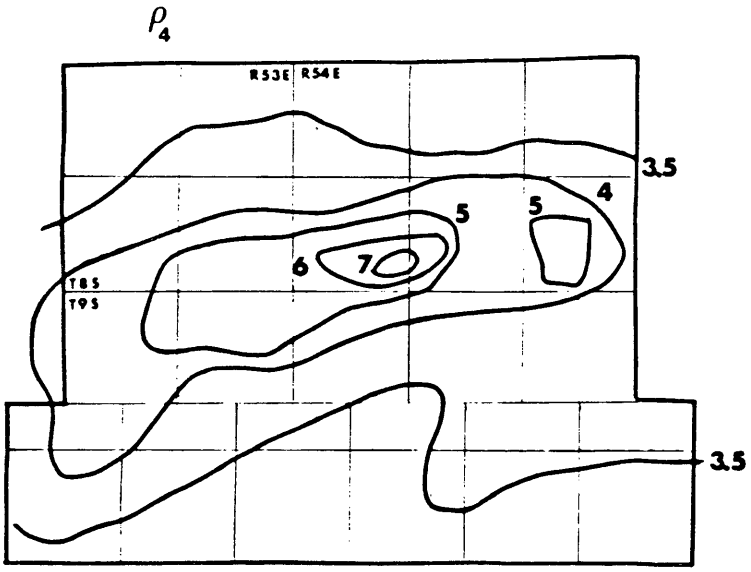

Figure 4. Average resistivity of geoelectric unit 4 from well log analysis.

The above analysis indicates generally decreasing resistivities down to the Muddy Sandstone and higher resistivities within the producing zone. Average resistivity for the section above the Muddy Sandstone is about 6 ohm-meters. Average resistivity of the producing zone appeared to be about 20-30 ohm-meters. The resulting transverse resistance contrast (T_2/T_1) is between 1.05:1 and 1.1:1. The anomaly sought at Belle Creek is on the order of only a few percent, at best.

Since the anomaly in apparent resistivity would be small, non-standard field procedures and interpretation techniques were used in an effort to emphasize any anomaly which might be present. Second vertical derivatives of the potential field were calculated in order to separate smaller anomalies from general trends. An inversion technique was used on the absolute potential to delineate relative strengths or polarities of dipole moments in elements of a grid in the subsurface.

Second vertical derivatives of the potential and the inversion technique appear to be able to delineate the thickest portions of the Muddy Sandstone within the survey area.

FIELD PROCEDURE

The bipole-dipole method consists of a stationary bipole current source with dipole receivers which measure potential differences at various locations around the source. The dipole receiver stations are commonly restricted to locations along the polar axis of the source bipole, polar bipole-dipole, or the equatorial axis of the source bipole, equatorial bipole-dipole surveys, to simplify geometric factors for apparent resistivity calculations. A modification of the unrestricted version of the bipole-dipole method was implemented for the survey in Belle Creek. Here two sources with a common central electrode oriented approximately perpendicular to each other, were employed. Both sources were approximately one mile long.

Dipole receiver stations consisted of four dipole receivers having a common ground at the center of the station. Dipole receivers were each 500 meters long. Receiver electrodes were porous, ceramic pots containing a copper electrode immersed in a copper sulfate solution. The recording truck was situated at the center of each station with the common electrode. The four dipoles were oriented, when possible, in two orthogonal directions. Each station had a common electrode position with some other station to enable calculation of absolute or "monopole" potentials to within

an unknown additive constant, one for each source used. Source and reciever locations are shown in figure 5.

The two current sources were employed independently, each for a period of five minutes. Current transmitted to the ground was in the form of an asymetric square wave to aid in polarity determination of measured potentials. The frequency used was low enough so that direct current could be assumed. Two sets of four potential difference measurements were obtained at each dipole receiver station using a four channel strip chart recorder. Each channel was connected to its own amplifier. Four different colors of wire and ink were used to distinguish records from different receiver legs. The relative direction of each leg was recorded along with color of wire and ink associated with each direction at every station. The amplifier gains associated with each channel were also recorded at this time. Time of each measurement was recorded to correlate with source current records containing transmission times and the source being used.

A station was occupied until a set of interpretable measurements were obtained having between ten and twenty cycles of the source for each leg of the receiver. The entire array was then moved to the next position, which was exactly one electrode length away from the end of the front

SOURCE AND RECEIVER LOCATIONS

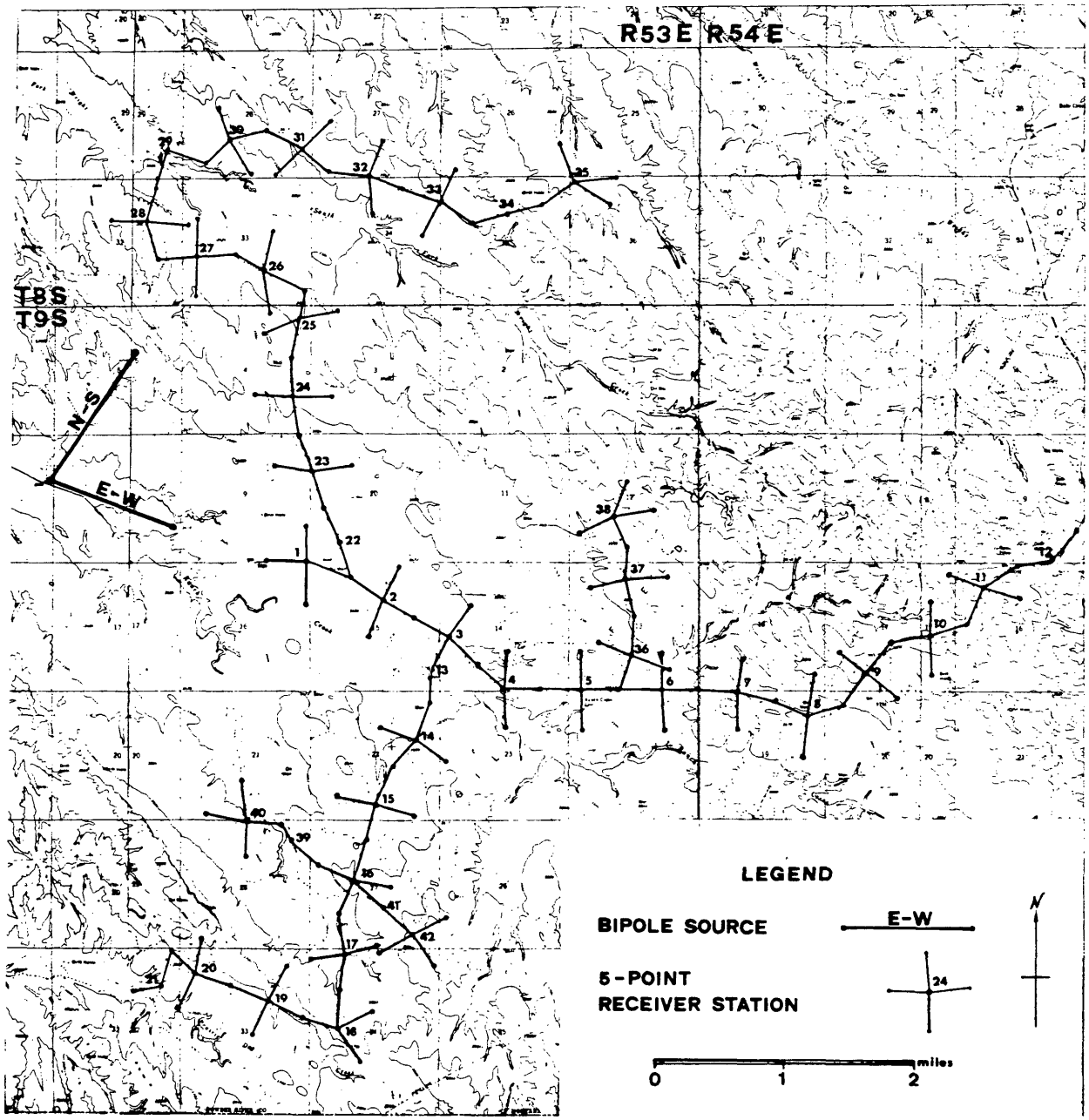

Figure 5. Topographic map of Belle Creek area showing source and receiver locations.

dipole array. By doing this, the front potential electrode from one station and the back potential electrode of the next station occupied the same point. The time required to pick up all equipment, move to the next station and lay out electrodes ranged from one hour, under ideal conditions, to several hours when complications arose. The use of a "trail bike" to lay out off road dipoles significantly reduced the time required to move to a new station and set up again.

The field crew consisted of only three people. One remained with the sources, turning them on every 20 minutes, for a period of five minutes respectively. The other two crew members obtained measurements at dipole receiver stations and moved the array to subsequent stations.

The field procedure could be improved by developing a system which does not allow interchangeability of amplifiers and recording channels. It would also help to have every part of each of the four recording systems blatantly color-coded to avoid any mixups, should repair be needed while in the field.

DATA REDUCTION

Measurements were repeated at each station for each source until approximately 10-20 cycles of the source current had been observed. Upon returning from the field, the average potential difference for each leg of each station was determined. A calibration factor was calculated for each amplifier from its response to a signal of a known strength. Potential differences were multiplied by their respective factors so that resulting potential differences were as if they were all recorded on the same system. The gain for each one was then removed.

A source current strength was then determined for each set of potential measurements by comparison of measurement times with transmission times on the source current records. These were generally around 90 amperes for the east-west source and 70 amperes for the north-south source. Potential differences measured were later divided by their respective current strengths to remove the effect of current strength from the data.

The base map containing source locations and electrode locations for each station was then digitized. The common electrode of the two sources was defined as the origin. X and y coordinates for the ends of the sources and receiver electrodes were determined.

A computer file was created containing the station numbers, the source strength, x and y coordinates of the five electrodes and four potential differences measured for each source at each station. This file was then used for all subsequent analysis of the data.

Signal strength ranged from tens of millivolts for stations near the source to tenths of millivolts for stations at large distances from the source. Potential differences were for the most part easily determined from field records. At points where the signal was not discernable, a value of .001 millivolts was assumed because values below .005 were not interpretable from the field records. This procedure was applied in few instances where the signal was too small to be seen.

In some instances it would have been helpful to have a gain between 10 or 100 on the amplifiers. At these times the signal strength was such that it was small but readable on the lower gain but too large to remain on scale for the higher gain.

An estimate of the standard deviation of the averaged potential differences measured was calculated for each measurement. The formula used was:

$$S = \sqrt{\frac{\sum x^2 - \sum (x/n)^2}{n-1}}$$

Where this is the standard deviation of the sample, it is related to the standard deviation of the population in the following manner (Hewlett Packard, 1976):

$$\sigma = \frac{S\sqrt{n-1}}{n}$$

Where: **S** is the standard deviation of the population,

σ is the standard deviation of the sample.

Standard deviations for potential measurements were generally on the order of about one percent of the value of the potential difference. On one or two occasions when the signal was strongly amplified, the standard deviations went up to ten or 20 percent of the observed values.

The data as used for further calculations are displayed in Appendix 1.

APPARENT RESISTIVITY

Bipole-dipole apparent resistivity values were calculated for four positions at each station. The method of calculation involved determining a total electric field magnitude for four different pairs of arbitrarily oriented measuring directions, and calculating apparent resistivity from the total field determined for each pair of measurements. Electric field components in arbitrary directions, as shown in figure 6, were approximated by dividing potential differences by the distances from the center electrode to each porous pot location.

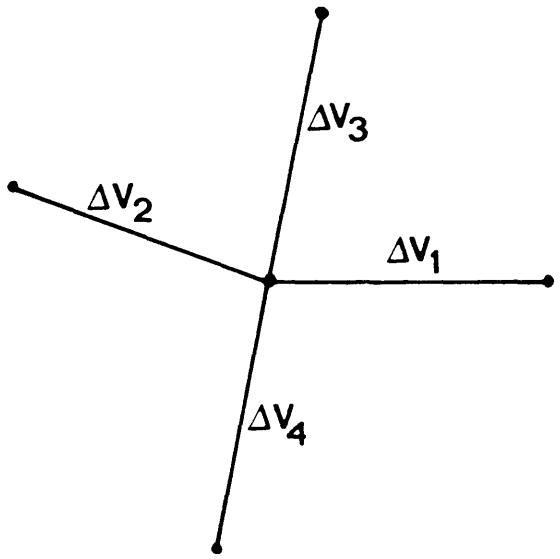

Figure 6. Potential differences measured by modified dipole receiver.

The formula used in total field calculations was:

$$ET = E1^2 + \frac{E2 - E1\cos\theta_1}{\sin\theta_1}$$

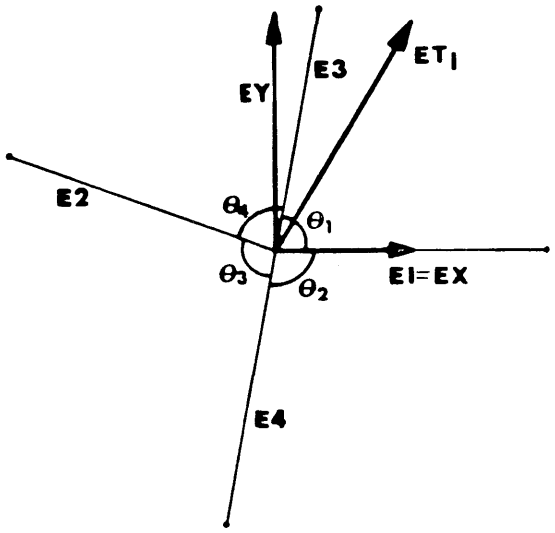

Figure 7. Determination of total electric field from adjacent components measured in arbitrary diversions.

Where E1, and E2, were adjacent values of the electric field components from V_1 and V_2 and θ_1 is the angle between adjacent potential difference measurements, as seen in figure 7.

Apparent resistivity was then calculated using the formula:

$$\rho_a = \left[\left[(YA/AO^3) - (YB/BO^3)\right]^2 + \left[(XA/AO^3) - (XB/BO^3)\right]^2\right]^{1/2} \frac{2\pi ET}{}$$

Where: AO is the distance from the center point of the station to the positive electrode of the source,

BO is the distance from the center point of the station to the negative electrode of the source,

YA is the Y-distance to the positive source electrode,

YB is the Y-distance to the negative source electrode,

XA is the X-distance to the positive source electrode,

XB is the X-distance to the negative source electrode. (Zohdy, 1978)

As is shown in Figure 8.

Each apparent resistivity was then plotted in its appropriate position on a map containing source and receiver locations for each of the two sources used (Figures 10 and 11). These values were then contoured by hand to see if any significant anomalies could be detected.

Several general patterns were noted on each map. The patterns which were observed can be most easily compared to the theoretical tendencies of apparent resistivity values computed for the case of a single layer with thickness equal to the length of the bipole source resting on an insulating basement (Figure 9). (Keller, and others, 1975) These include: 1) relatively low values of apparent resistivity near the polar axis of the source and 2) increasing apparent resistivities with increasing distance from the source.

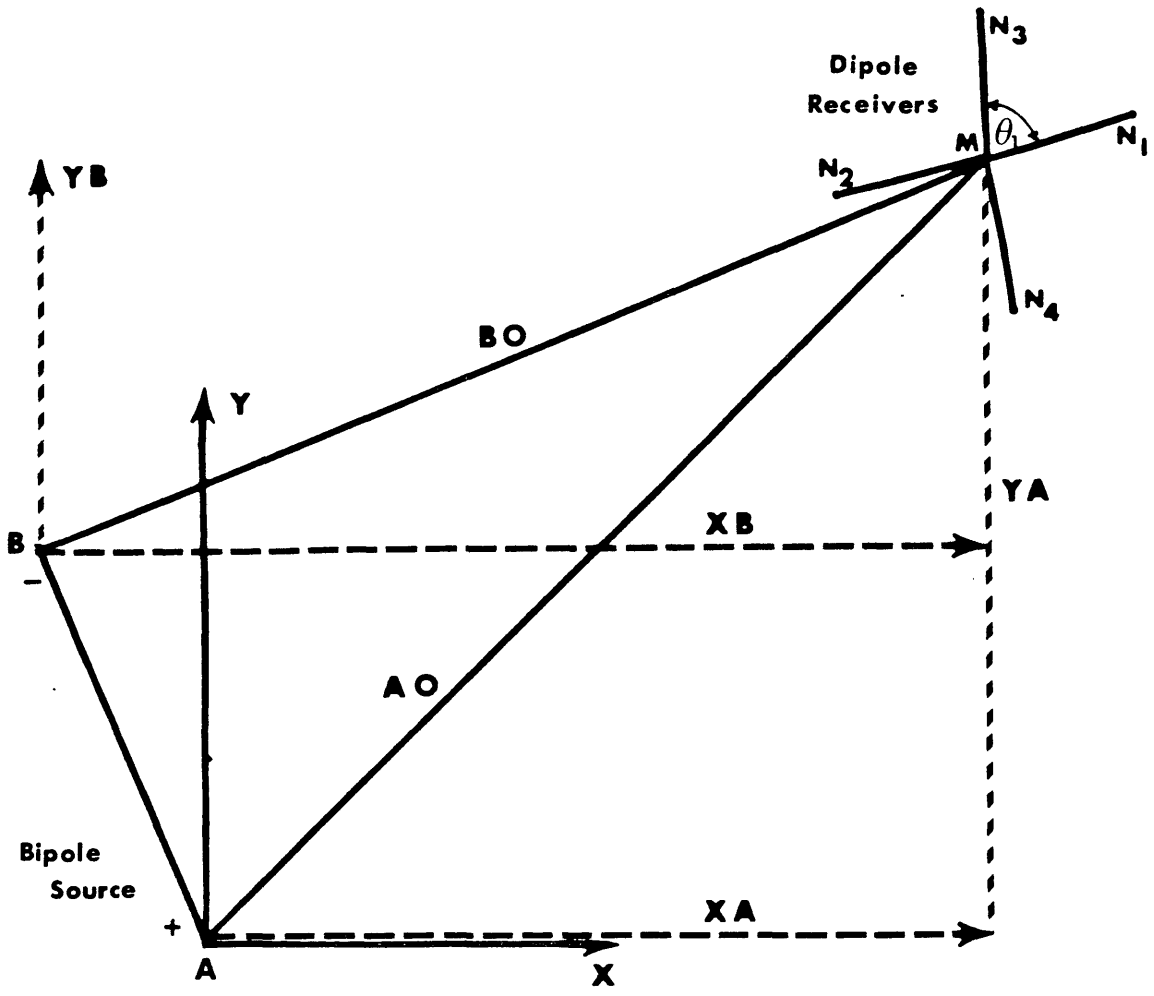

Figure 8. Source-receiver geometry, for calculation of geometric factor in apparent resistivity determination.

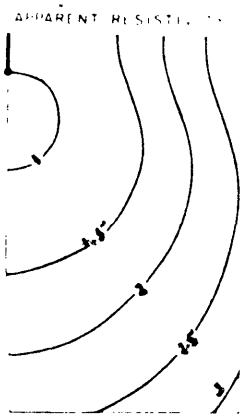

Figure 9. Contour map of apparent resistivity for a single layer over a resistive basement. Thickness of the surface layer is equal to the length of the bipole source and its resistivity is equal to 1 ohm-meter. Basement is infinitely thick, with infinite resistivity.

Anomalously high apparent resistivities can be observed on the extreme eastern portion of the apparent resistivity maps for both sources. The contours in this area closely follow the general trend of the topographic contours of the hill upon which station 9 was located. The anomaly is half as large on the map of apparent resistivities of the East-West source. The North-South source is oriented in a near perpendicular direction to this particular topographic feature and the East-West source is oriented in a near parallel direction. Relative current directions from the two differently oriented sources could be the reason for the larger magnitude of the anomaly for the North-South source.

The small area in the central portion of the apparent resistivity map for the North-South source with apparent resistivities above 30 ohm-meters is due to lack of signal from one leg of station 36. In this case a value of .001 millivolts was assumed for the west leg, compared with signals of about .5 millivolts for the other three legs of this station. When combined with voltages measured in other directions at this station, this would give rise to two high resistivities associated with the west leg of this station.

An anomaly due to a thin resistive layer could not be readily interpreted from these maps. There are irregularities of the contours in the south eastern portion of the maps which might be due to thick accumulations of Muddy Sandstone (figure 15), but it would be difficult to interpret these irregularities as oil deposits rather than noise or near surface resistivity contrasts.

The presence of pipelines in the study area might be a cause of concern. Since the bipole-dipole method is reputed to be very sesitive to shallow inhomogeneities,(Dey and Morrison, 1977) the pipelines should appear as apparent resistivity lows on the bipole-dipole apparent resistivity maps. These did not appear. This might be due to the long dipole length used for measurements, or a smaller effect than might be expected from the pipelines in the area.

APPARENT RESISTIVITY

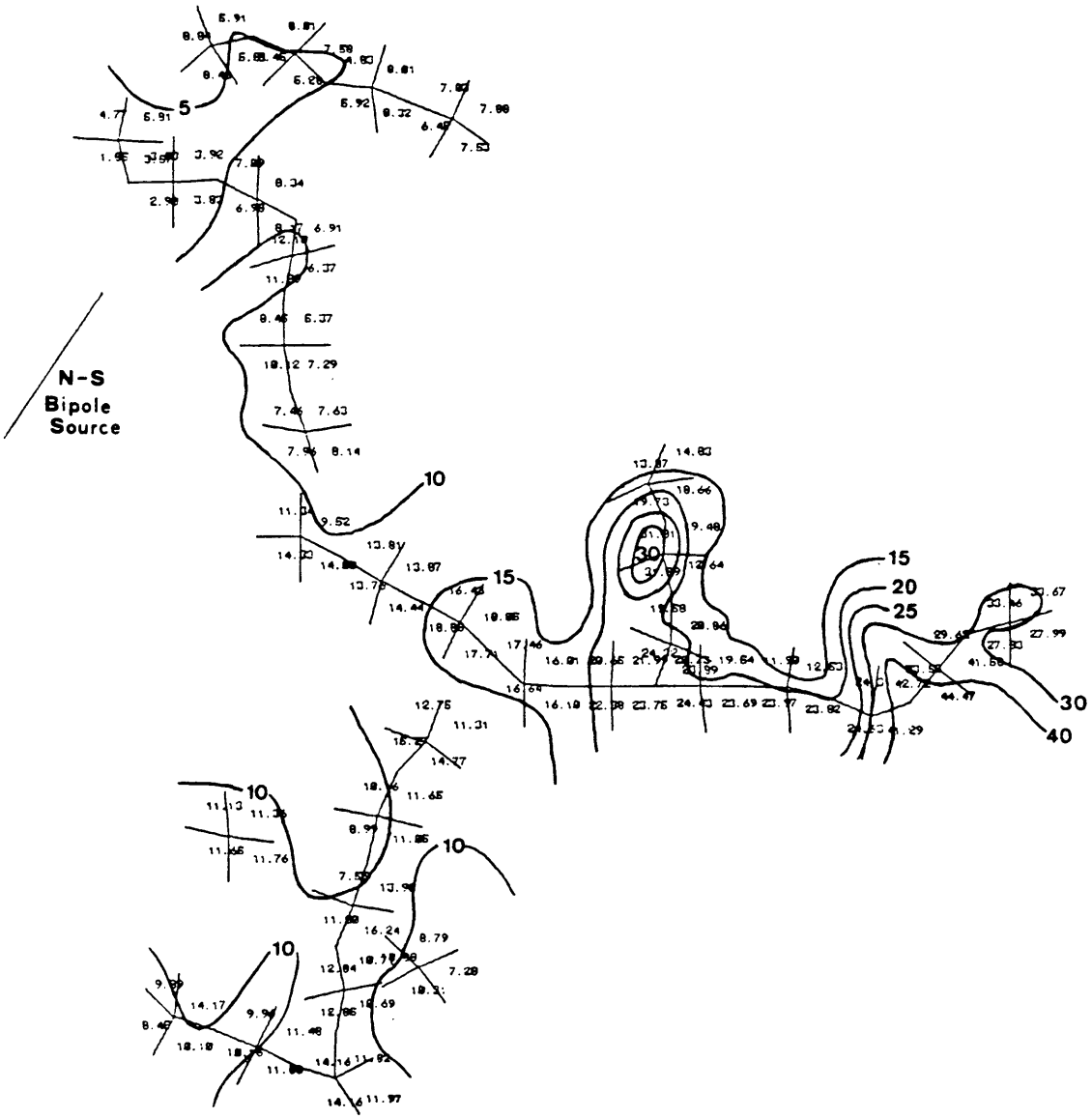

Figure 10. Apparent resistivity map for the North-South bipole source.

APPARENT RESISTIVITY

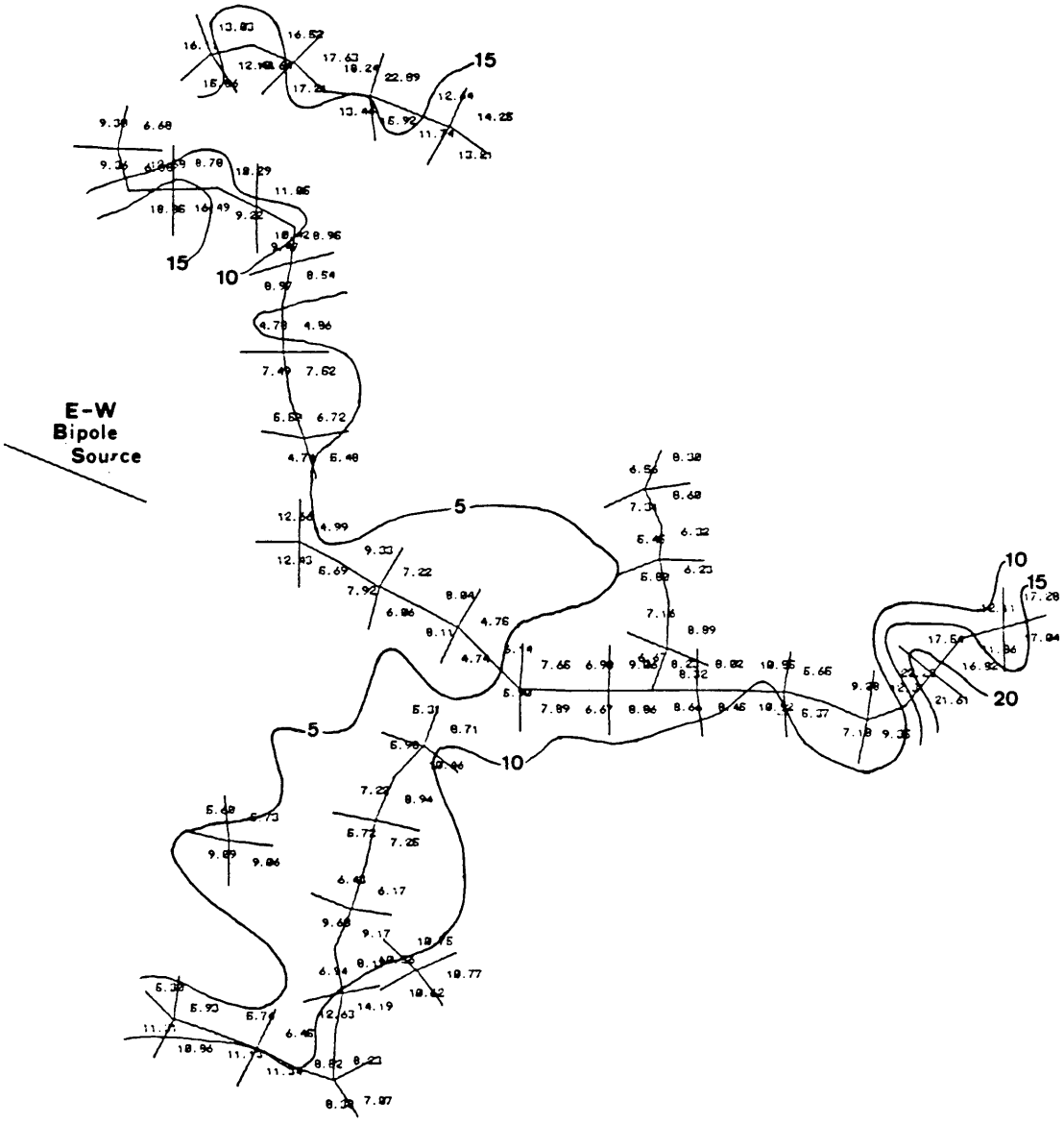

Figure 11. Apparent resistivity map for the East-West bipole source.

SECOND VERTICAL DERIVATIVES OF THE POTENTIAL FIELD

Potentials and second vertical derivatives of the potential due to a thin resistive layer of finite extent within a layered medium were calculated using a program developed by Whan,(1979). Results from calculations on several models with different transverse resistance constants indicate second vertical derivatives of the potential can define a thin resistive layer in the subsurface.

Features of second vertical derivative maps from these models include a positive anomaly due to the body but offset from the center in a direction away from the source. Derivatives in remaining portions of the grid are negative. Models utilizing transverse resistance contrasts of 2:1 or greater, showed positive anomalies due to a thin resistive layer within the grid used for calculations. A model using a transverse resistance contrast of .3:1 showed no closed positive areas.

A model of the Belle Creek oil field was prepared. Two truncated ellipses were used as models for the two isolated areas in which the Muddy Sandstone thickness is greater than 6 meters (20 feet), within two layers with resistivities equal to 6 ohm-meters. The depth of these bodies was 1.2 kilometers. For this model a transverse resistance contrast of 3:1 was needed for positive anomalies of the second vertical derivatives to be detected on the surface.

The second derivative of the potential field was estimated at each station having four legs. These calculations were based on the assumption that the field is stationary, therefore, Laplace's equation is valid within the region under consideration. Two conditions must be met for this assumption to be valid. The first is that there are no net charge accumulations within the region and the second is the frequency of the current in the source be sufficiently low that direct current may be assumed. Laplace's equation may be written as:

$$\nabla^2 U = \frac{\delta^2 U}{\delta x^2} + \frac{\delta^2 U}{\delta y^2} + \frac{\delta^2 U}{\delta z^2}$$

Or:

$$-\frac{\delta^2 U}{\delta z^2} = \frac{\delta^2 U}{\delta x^2} + \frac{\delta^2 U}{\delta y^2}$$

The second derivatives in the horizontal directions were approximated in the following manner. First derivatives of the potential field in the direction of measurement are the electric fields described above, figure 12. These components were then resolved into two sets of orthogonal components. One set with its x-axis in the direction of ΔV_1, and the other set with its x-axis in the direction of ΔV_2 (figure 12).

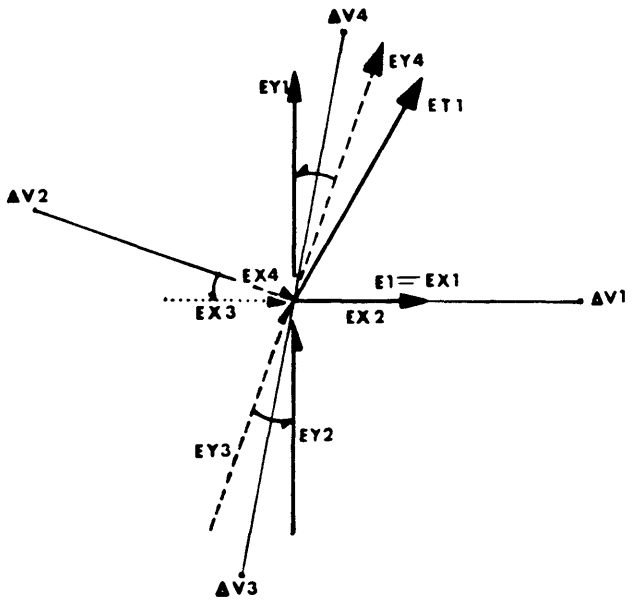

$$EY1 = \frac{E3 - E1\cos\theta_1}{\sin\theta_1} \qquad EX1 = ET1\cos(\pi/2 - \theta_1)$$

$$EY2 = \frac{E4 - E1\cos\theta_2}{\sin\theta_2} \qquad EX2 = ET2\cos-(\pi/2 - \theta_2)$$

$$EY3 = \frac{E4 - E2\cos\theta_3}{\sin\theta_3} \qquad EX3 = \left[ET3\cos(\pi/2 - \theta_3)\ \cos(\theta_2 + \theta_3)\right]$$

$$EY4 = \frac{E3 - E2\cos\theta_4}{\sin\theta_4} \qquad EX4 = \left[ET4\cos(\pi/2 - \theta_4)\ \cos(\theta_1 + \theta_4)\right] .$$

Figure 12. Total field components resolved into two sets of orthogonal components.

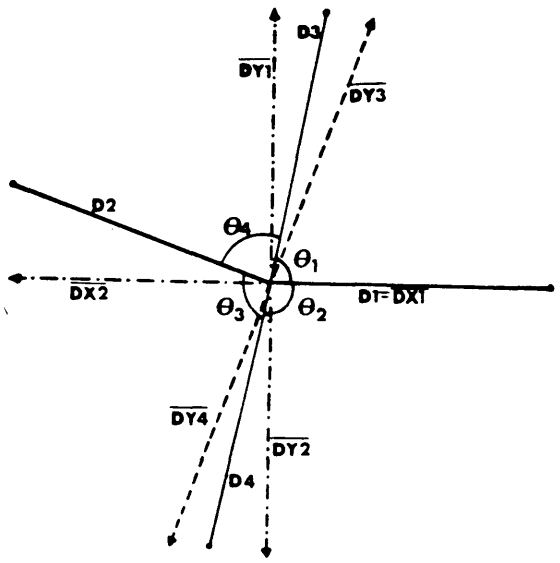

Y Distance

$$DY1 = D3 \sin\theta_1$$

$$DY2 = D3\sin\theta_1 + D2\sin\left(\theta_1 + \theta_4\right)$$

$$\overline{DY1} = \left(DY1 + DY2\right)/2$$

$$DY3 = D4 \sin\theta_2$$

$$DY4 = D4\sin\theta_1 + D2\sin\left(\theta_2 + \theta_3\right)$$

$$\overline{DY2} = \left(DY3 + DY4\right)/2$$

$$\overline{DY} = \left(\overline{DY2} + \overline{DY1}\right)/2$$

X Distance

$$\overline{DX1} = D1$$

$$DX3 = D2\cos\left(\theta_1 + \theta_4\right) + D4\cos\theta_2$$

$$DX4 = D2\cos\left(\theta_2 + \theta_3\right) + D3\cos\theta_1$$

$$\overline{DX2} = \left(DX3 + DX4\right)/2$$

$$\overline{DX} = \left(\overline{DX1} + \overline{DX2}\right)/2$$

Figure 13. Electrode lengths projected on to same set of orthogonal coordinates as electric field components.

Electrode lengths were projected onto the same set of orthogonal directions and an average length determined in each direction. Second derivatives were then determined by finding the difference between the electric field components in the X and Y directions, respectively and dividing by the average distances in the respective directions. These were then added together to give an approximation of the negative of the second vertical derivative of the potential, as shown below.

$$\frac{\delta^2 U}{\delta x^2} = \frac{\delta E}{\delta x} \approx (EX1 + EX2)/DX$$

$$\frac{\delta^2 U}{\delta y^2} = \frac{\delta E}{\delta y} \approx (EY1 + EY2)/DY$$

$$\therefore \quad -\left(\frac{\delta^2 U}{\delta x^2} + \frac{\delta^2 U}{\delta y^2}\right) = \frac{\delta^2 U}{\delta z^2}$$

Interpretation of vertical derivatives as outlined by Peters, (1949) is essentially qualitative in nature, the main use being to separate smaller anomalies from general trends in the survey area. These smaller features may be identified by a change in curvature of the field which is more pronounced in the second derivatives. Under certain

conditions the lateral extent of an anomalous body can be determined from the zero contour of the second vertical derivatives of a potential field. This condition is that the contact of the body is greater than one depth of burial away from the center of the body.

A second derivative map was prepared for each source for the Belle Creek Bipole-Dipole Survey, (Figures 13 and 14). These exhibit some encouraging results, the most interesting being closed positive anomalies over the thickest portions of the Muddy Sandstone and existing oil production, (Figures 14 and 15). Average radii of the closed contours indicate that they might be from a body which lies at a depth less than 1.4 kilometers (4800 feet). Production in this area comes from depths between 1.3 kilometers (4300 feet) and 1.37 kilometers (4500 feet). The area of the anomalies for both sources, is about 2.5 square kilometers as is the area of portions of the Muddy Sandstone with thickness greater than 20 feet, thought to cause these anomalies. One feature noted on both maps is that the anomalies in the second derivatives are displaced from the thickest portion of the Muddy by a distance of about one mile away from the current source.

The reason for the offset of the anomalies is probably due to the fact that the electric field and equipotential lines will be distorted by a body having a different resistivity than the surrounding medium, this distortion would be

VERTICAL DERIVATIVES

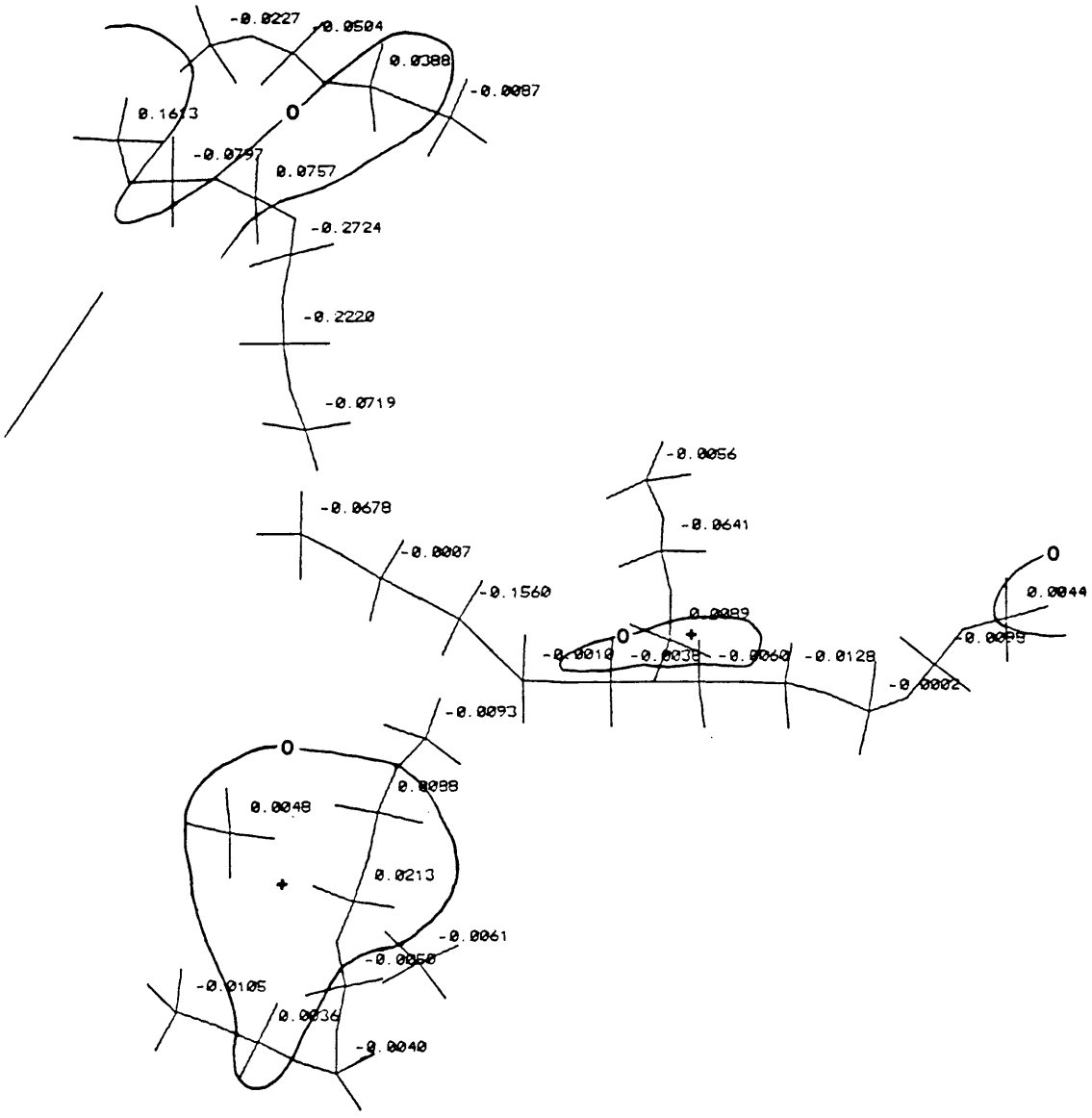

Figure 14. Second vertical derivative of the potential map for the North-South bipole source.

VERTICAL DERIVATIVES

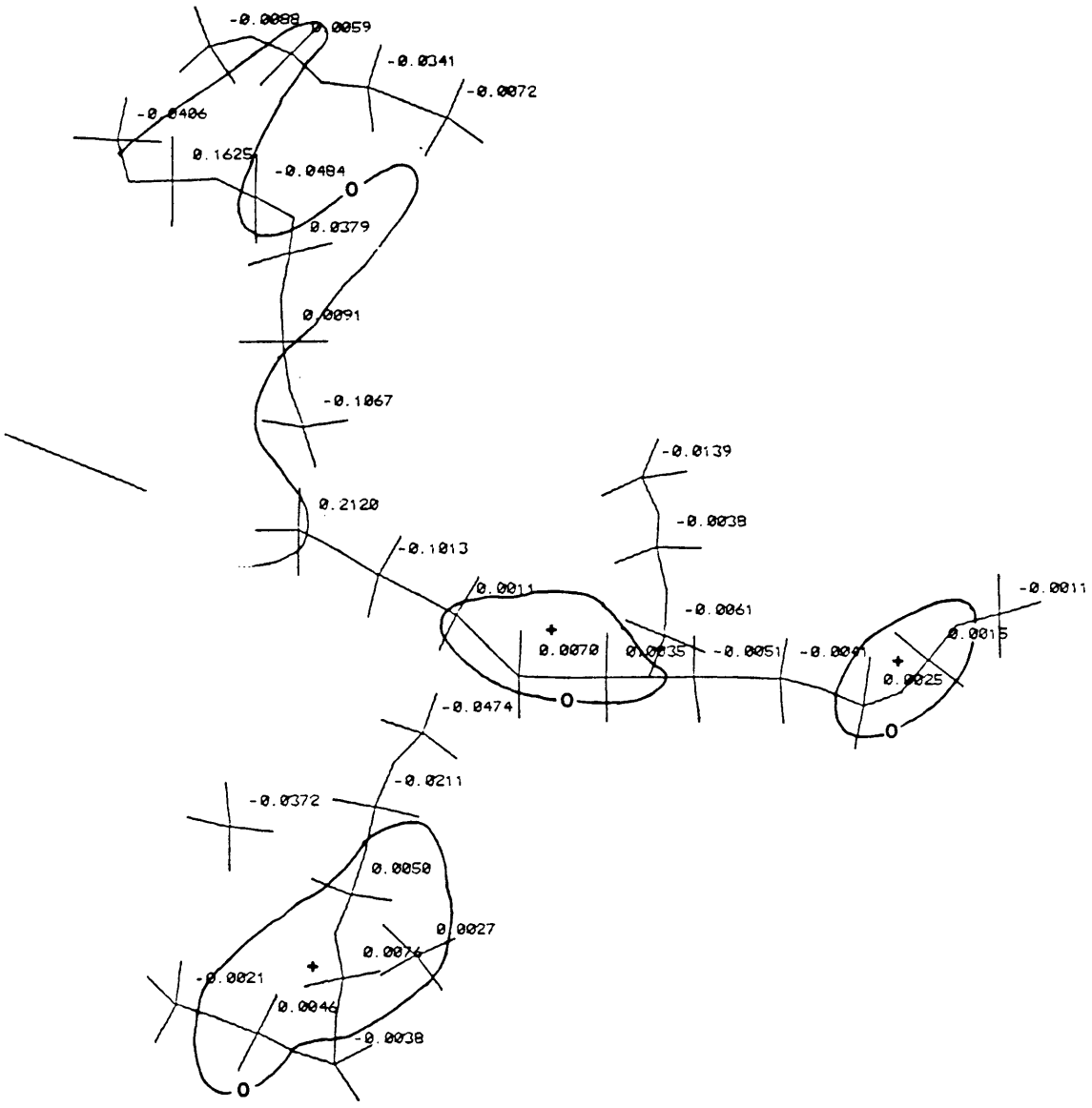

Figure 15. Second veritcal derivative of the potential map for the East-West bipole source.

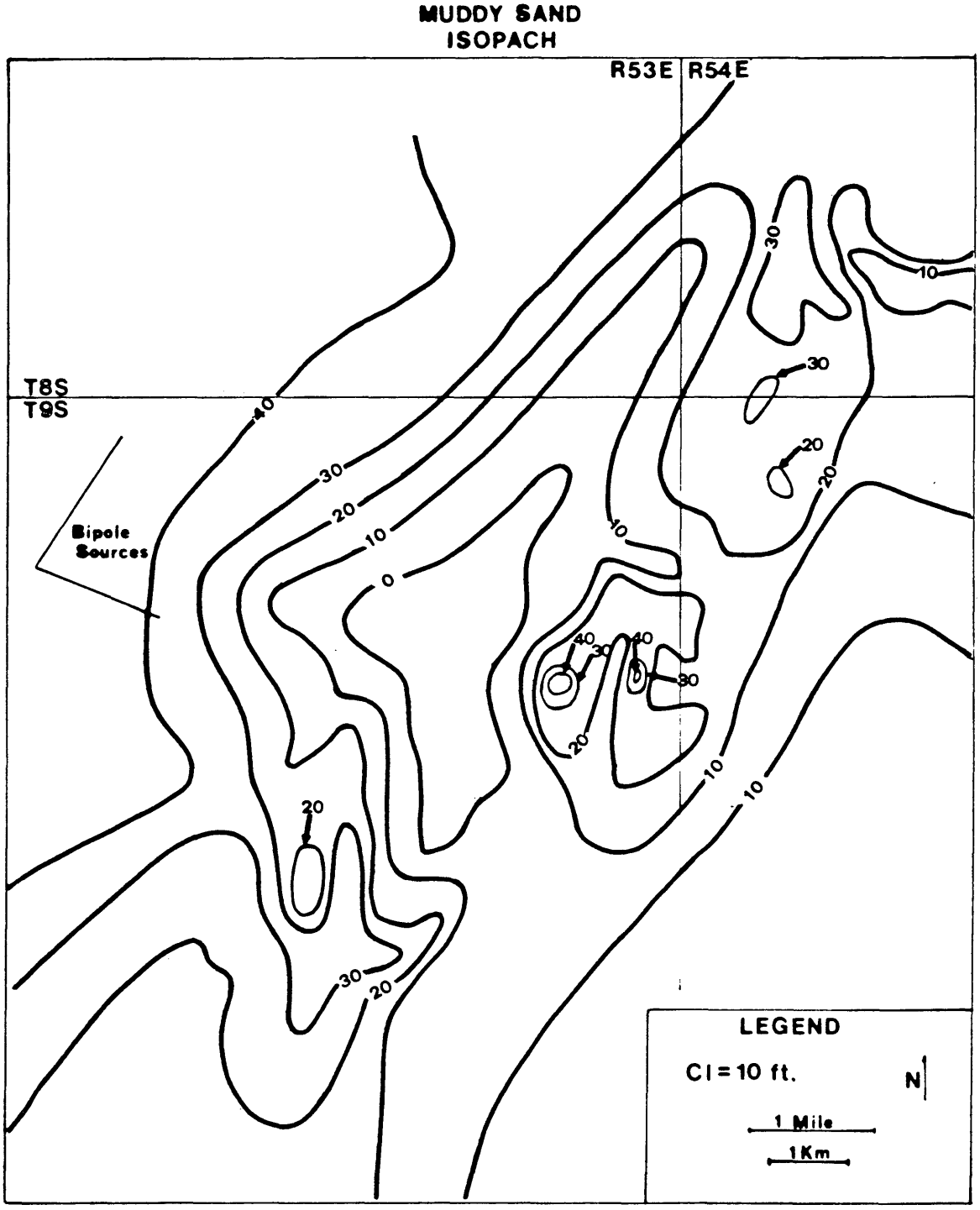

Figure 16. Muddy Sandstone isopach map.
After McGreogor and Biggs (1968)

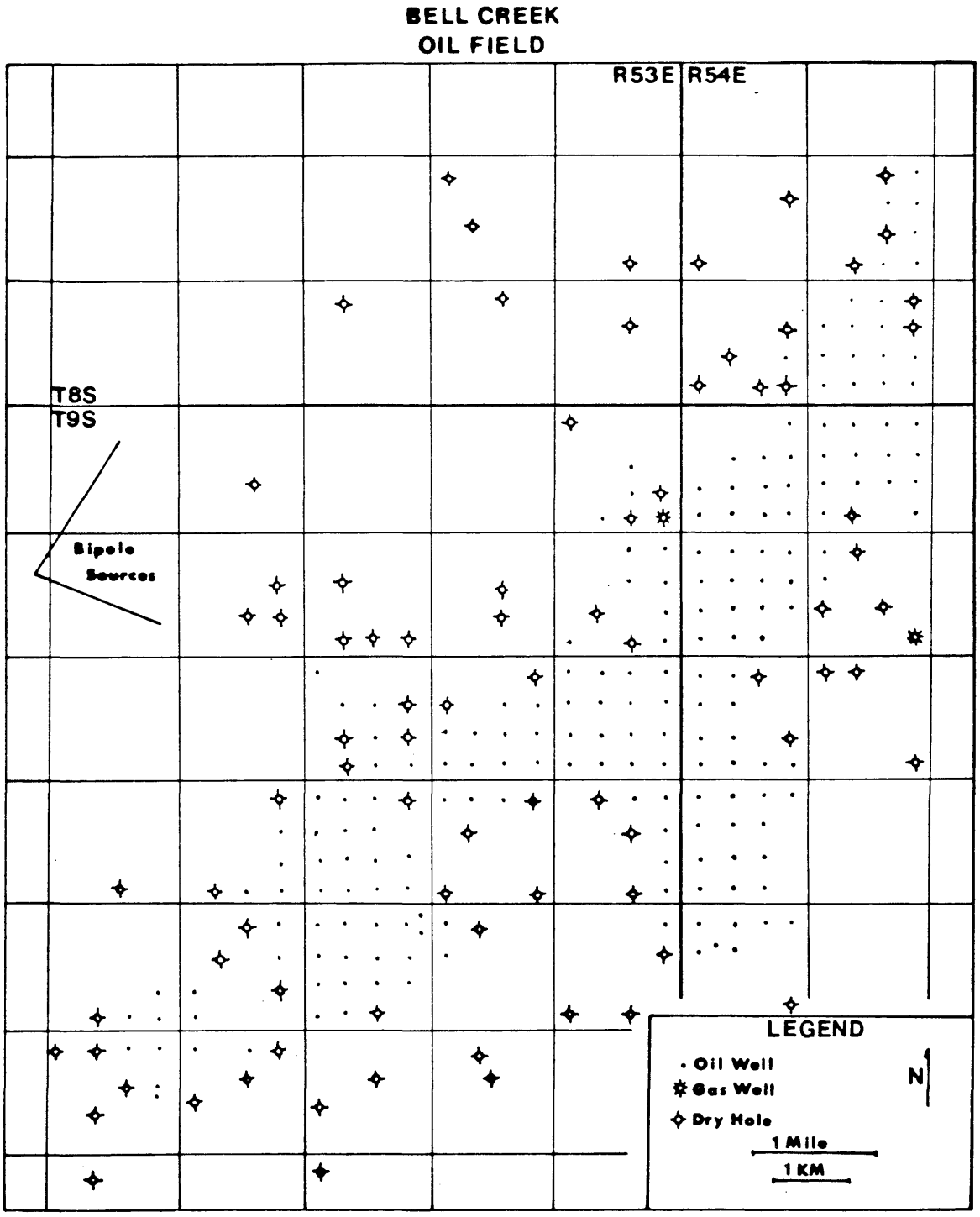

Figure 17. Bell Creek oil field map. After McGreogor and Biggs (1968).

greatest near the edge farthest away from the source. The anomalous curvature of equipotential lines due to the presence of the body would occur in this area and be defined by the second derivatives of the potential field.

Another anomaly is also present on both maps in the western portion of the survey area. These can also be correlated with greater thicknesses of the Muddy Sandstone. These anomalies are also displaced away from the source by about one mile. The shape of these anomalies does not correlate with the shape of the isopachs of the Muddy with which they are associated. They are also different in size as one compares from map to map. This phenomena might be due to the fact that all of the derivatives are close to zero in this area and the actual zero contour could be anywhere within a range of two to three stations. The values below .001 on the maps are below the measuring capabilities of the instruments and should probably be called zero. This would increase the area of these two anomalies and make them correlate with the observed geology to a higher degree.

Another positive anomaly is present on the extreme eastern portion of the map of second vertical derivative from the north-south source. This anomaly can be correlated with the apparent resistivity high in the same area, which is thought to be caused by topography.

The anomalies seen on these two maps are similar to those produced by modeling of Belle Creek by Whan (1979). The fact that a much higher transverse resistance was needed to produce anomalies than what appears to be presesent from well log analysis is disturbing. The problem might lie in oversimplification of the model to facilitate calculation of the foward solution, underestimation of the resistivity of the producing zone, or some combination of both. Underestimation of the resistivity of the producing zone is probable for several reasons. The resistivity of the producing zone will be lowered by the introduction of low resistivity drilling mud into the permiable resevoir rock surrounding the borehole. In conjunction with the above effect, the true resistivity of a highly resistive zone which is thinner than the electrode spacing of the logging tool will be underestimated. Further reasearch to better integrate the forward modeling problem and the field results is necessary.

INVERSION OF MONOPOLE POTENTIAL

The potential differences which were measured at each station for both sources were converted to a single monopole potential in the following manner. The potential differences were added together for each station along a continuous line. A correction term was then determined which when added to the sum at the point farthest from the bipole source would produce a potential of zero at a great distance away from the source. The partial sum at each point after addition of the correction term would then be the absolute potential as refered to a point at infinity.

The potentials determined in this manner were then combined into one potential which might have been measured with one bipole pointing towards the observation point. This was done in order to minimize effects due to lateral changes of resistivity in near surface rocks, (Keller and Furgerson, 1977). The effect of source orientation can be seen in the anomaly produced by a hill on the apparent resistivity maps, Figures 10 and 11. The anomaly is readily apparent when the source is perpendicular to the strike and the body and is less apparent when the source is parallel to the strike of the body.

An inversion technique was applied which would assign magnitudes and directions to dipole moments on a grid at a given depth in the subsurface. The magnitudes of the individual dipole moments were such that the combined effect of

all of the moments would give rise to the potential at each observation point on the surface.

The criterion for fit was a minimization of the least squares error between the potentials due to dipole moments and observed potentials. The forward portion of the problem was formulated in the following manner.

A grid at a given depth was prepared having a number of elements each of which had a dipole moment associated with it (Figure 18). The potential due to a dipole at a distance can be written as:

$$V(r)=\frac{\vec{P}\cdot\vec{r}}{4\pi r^3}$$

Where $\vec{P}$ is the vector dipole moment
and $\vec{r}$ is the vector directed from the center of the dipole to the observation point.

If P is replaced by a surface distribution of dipole moment and assumed to remain constant over the area under consideration, the potential due to the vertical component of this surface distribution of moment can be written as:

$$V(r) = \frac{P_z}{4\pi}\int_{Area} \frac{z}{(x^2+y^2+z^2)^{3/2}}\, dA$$

At each observation point on the surface the potential is the potential due to all of the dipole moments on the grid.

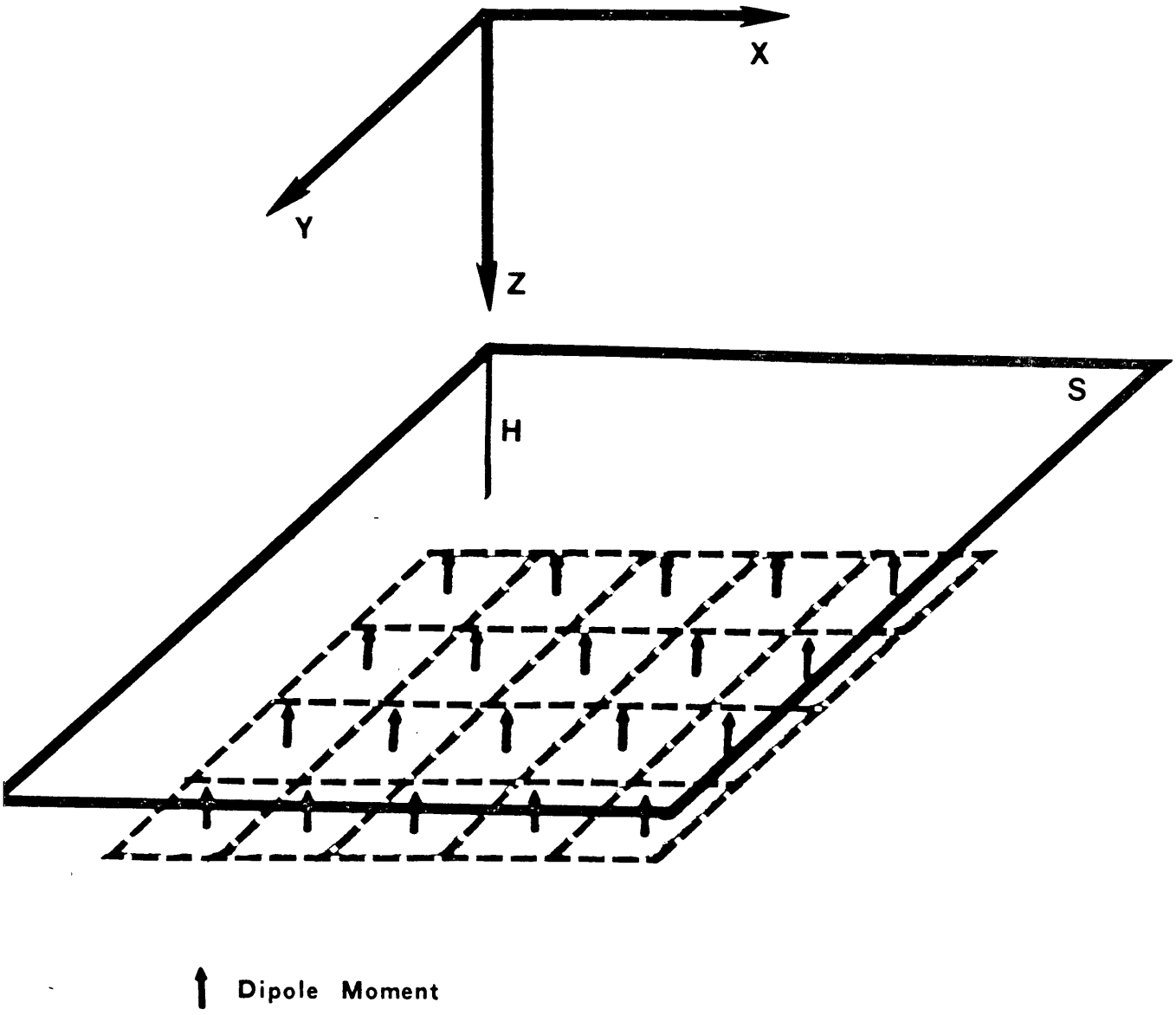

Figure 18. Grid arrangement for inversion of Monopole Potential. Potentials on the surface (S) will be due to the combined effect of all dipole moments on the grid.

This can be expressed as:

$$V_i = \sum_{j=1}^{NP} \frac{P_j}{4} \int_{Area} \frac{z_{ij}\, dA}{(x_{ij}^2+y_{ij}^2+z_{ij}^2)} \quad ;i=1,NOBS$$

Where x_{ij} is the x distance between the j^{th} element and the i^{th} observation point and y_{ij} is the y distance between the j^{th} element and the i^{th} observation point.

The combined effects of all potentials, normalized by their individual currents, may be written as a matrix equation as follows:

$$\begin{bmatrix} V_1 \\ V_i \\ V_{NOBS} \end{bmatrix} = \begin{bmatrix} A_{1,1} & \cdots\cdots & A_{1,NP} \\ A_{i,1} & \cdots\cdots & A_{i,NP} \\ A_{NOBS,1} & \cdots\cdots & A_{NOBS,NP} \end{bmatrix} \begin{bmatrix} P_1 \\ \\ P_{NP} \end{bmatrix}$$

Where $V_{1,NOBS}$ are the observed potentials,

$P_{1,NP}$ are the dipole moments sought,

and $A_{1,1}$; $A_{NOBS,NP}$ are the coefficients obtained from the integration described above.

Subsequently the potentials from the two different sources were combined into one potential which might have been measured with one source bipole pointing towards the observation point, (Figure 19). The potential in a uniform half space, due to a source of this type can be written as:

$$V_0 = \frac{\rho_0}{2\pi} \left[\cos\beta_1 (1/R-1/R_1)+\cos\beta_2 (1/R-1/R_2)\right]$$

Where R is the distance from the common central electrode of the source to the observation point, R_1 is the distance from the positive electrode of one source to the observation point and R_2 is the distance from the positive electrode of the other source to the observation point. β_1 and β_2 are the angles between R_1 and R and R_2 and R respectively. The cosines of β_1 and β_2 were then multiplied by the additive constants which were determined to reduce the potential differences to absolute potentials.

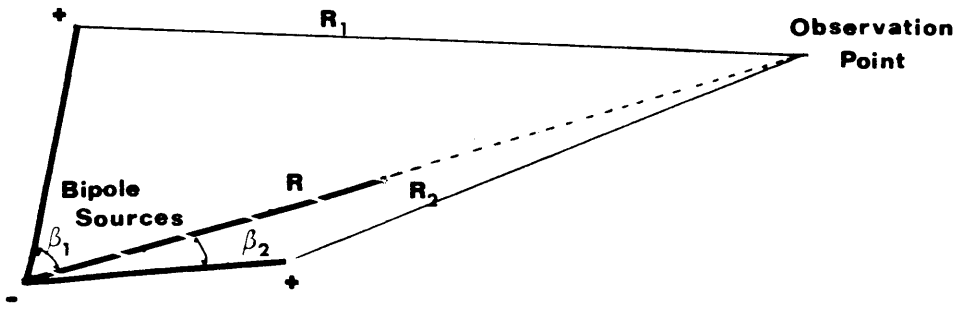

Figure 19. Potential for uniform half space due to single source pointing towards each observation point.

The described source rotation procedure was then incorporated into the system of equations describing the field in the following manner.

$$\begin{bmatrix} V_1 \\ \cdot \\ \cdot \\ \cdot \\ \cdot \\ \cdot \\ \cdot \\ V_{NOBS} \end{bmatrix} = \begin{bmatrix} A_{1,1} & \cdots & A_{1,NP} & B_1 & B_2 & A_\rho \\ \cdot & & & \cdot & & \\ \cdot & & & \cdot & & \\ \cdot & & & \cdot & & \\ \cdot & & & \cdot & & \\ \cdot & & & \cdot & & \\ \cdot & & & \cdot & & \\ A_{NOBS,1} & \cdots & A_{NOBS,NP} & & & \end{bmatrix} \begin{bmatrix} P_1 \\ \cdot \\ \cdot \\ P_{NP} \\ P_{C1} \\ P_{C2} \\ \rho_0 \end{bmatrix}$$

Where ρ_0 is the coefficient of the apparent resistivity of a uniform half space as shown below.

$$A_\rho = 1/2\pi\left[B_1(1/R-1/R_1)+B_2(1/R-1/R_2)\right]$$

where B_1 and B_2 are the cosines of the angles β_1 and β_2 described above. By incorporating these three terms (B_1C_1, B_2C_2, A_ρ) into the system of equations, the effect of the primary field will be removed from the potentials observed.

If the above matrix were square and non-singular, inversion to the necessary dipole moment strengths and apparent half space resistivity would consist of simple matrix inversion, as shown below.

$$[P] = [A]^{-1}\,[V]$$

Where P is the vector consisting of the dipole moments, additive constants, and uniform half space resistivity

sought, $[A]$ is the coefficient matrix, and $\vec{V}$ is the vector containing the observed potential values.

Since the matrix was overdetermined, having more equations than unknowns, a more complicated procedure was required. First the matrix was multiplied by its transpose to make it square. Then a damping factor was added to elements along the diagonal to insure non-singularity of the resulting matrix. This process of adding small constants along the diagonal is known as Ridge Regression (Stoyer,1978). In operator notation this process this process can be expressed as:

$$\vec{P} = \left[A^T A + k^2 I\right]^{-1} A^T \vec{V}$$

where: A^T is the transpose of the coefficient matrix A, k is the damping factor, and I is the identity matrix.

Inversion of the coefficient matrix was accomplished through a singular value matrix decomposition technique developed by Golub and Reinsch (1970), programed by R. C. Singleton, and later translated to Fortran IV by J. G. Lewis (1973). It decomposes the coefficient matrix $[A]$, into an m x n orthogonal matrix $[U]$, an n x n orthogonal $[V]$, and an n x n diagonal matrix $[S]$ containing the singular values such that:

$$[A] = [U]\,[S]\,[V^T]$$

Where: $[U]$ consists of n orthonormalized eigen vectors with the n largest eigen values of A^TA ,

$[V]$ consists of the orthonormalized eigen vectors of $[A^TA]$,

and $[S]$ consists of a diagonal matrix of the non-negative square roots of the eigen values of A^TA.

The psuedo inverse of A is then:

$$[A]^{-1} = [V] [S] [V^T]$$

The three portions of the coefficient matrix are then combined with a given damping factor through several intermediate steps to produce dipole moments for that specific damping factor. The last three terms in the resulting vector P are the two additive constants normalized by their respective rotation cosines, and the apparent half space resistivity of the medium required to produce the primary field.(Stoyer, 1979)

Potentials were then calculated at each observation point due to the derived dipole moments and uniform half space terms. The square root of the sum of the squared error at each observation point was then normalized by the number of observations made.

Several damping factors were tried and the normalized amplitude of the error for each damping factor was plotted as a function of the damping factor. This procedure

typically results in a curve similar to the one shown below (Figure 20).

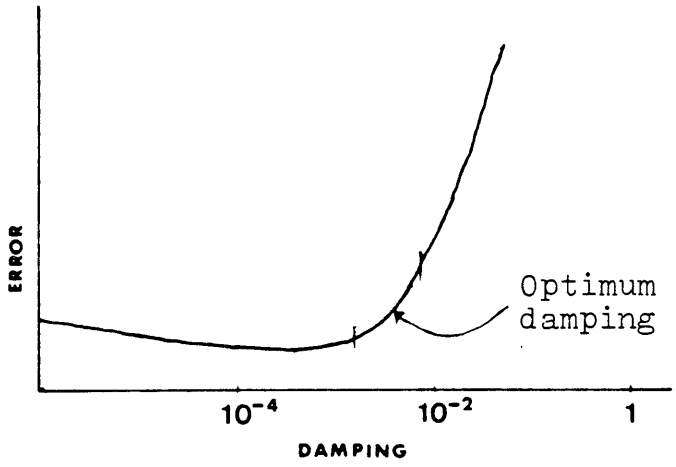

Figure 20. Typical error versus damping curve for inversion procedure.

For this analysis the minimum was not apparent on the left side of the curve. Inversion of theoretical data, with added noise, indicates the optimum choice for a damping factor lies within the range where the curve begins to ascend rapidly. Within this range, the values resulting from inversion correlate best with the values known in advance (Stoyer,1979). The area in which the curve begins to rise rapidly indicates that the damping factor is being given priority over the observations by the inversion process. Subsequently important information contained in the data will be ignored.

RESULTS OF INVERSION OF THEORETICAL MODEL

This inversion technique was applied to a theoretical model of a thin resistive layer. At a depth of approximately 1 kilometer, the ratio between the transverse resistance of the thin layer and an otherwise uniform half space (T_2/T_1) .3:1. The resistivity of the uniform space was given as 1 ohm-meter. Inversion of this model indicated that positive dipole moments arise where the thin resistive body occurs but change signs where there is no body, Figure 22. Apparent resistivity of the uniform half space as a result of inversion was within the range of 1.00 and .858 for different damping values. Dipole magnitudes in this case ranged from $+10^{-2}$ over the center of the body to -10^{-4} off the edge of the body. There also appeared to be a distinct positive influence due to the source. The high positive values on the left side of the grid are most likely due to the proximity and polar orientation of one of the sources in this model. Non-symmetry of the inversion results can be attributed to the lack of symmetry in the source placement for the model. The two additive constants which came out of the inversion were generally 1-2 orders of magnitude smaller than the dipole moments resulting from inversion. The magnitude of the anomaly in this case was generally less than two percent of the primary field. The optimum value of damping in this case was chosen between 1×10^{-2} and 3×10^{-2}, Figure 21.

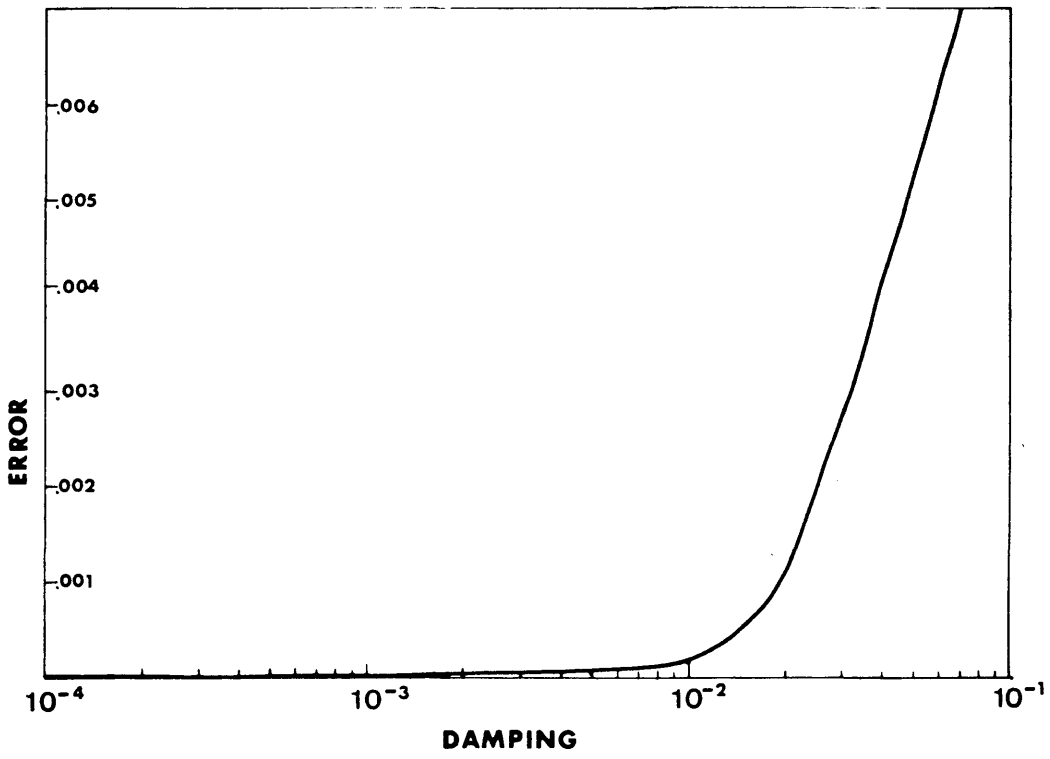

Figure 21. Error versus damping curve for inversion of thin resistive layer model. Depth is 1 kilometer. Transverse resistance contrast (T_2/T_1) is .3:1.

Plots of these results compared with the body dimensions indicate that the inversion technique is capable of delineating a thin resistive body at a depth of 1 kilometer when the grid exactly underlies the observation points and the observations are completely noise free, or will indicate general behavioral characteristics of the inversion technique applied.

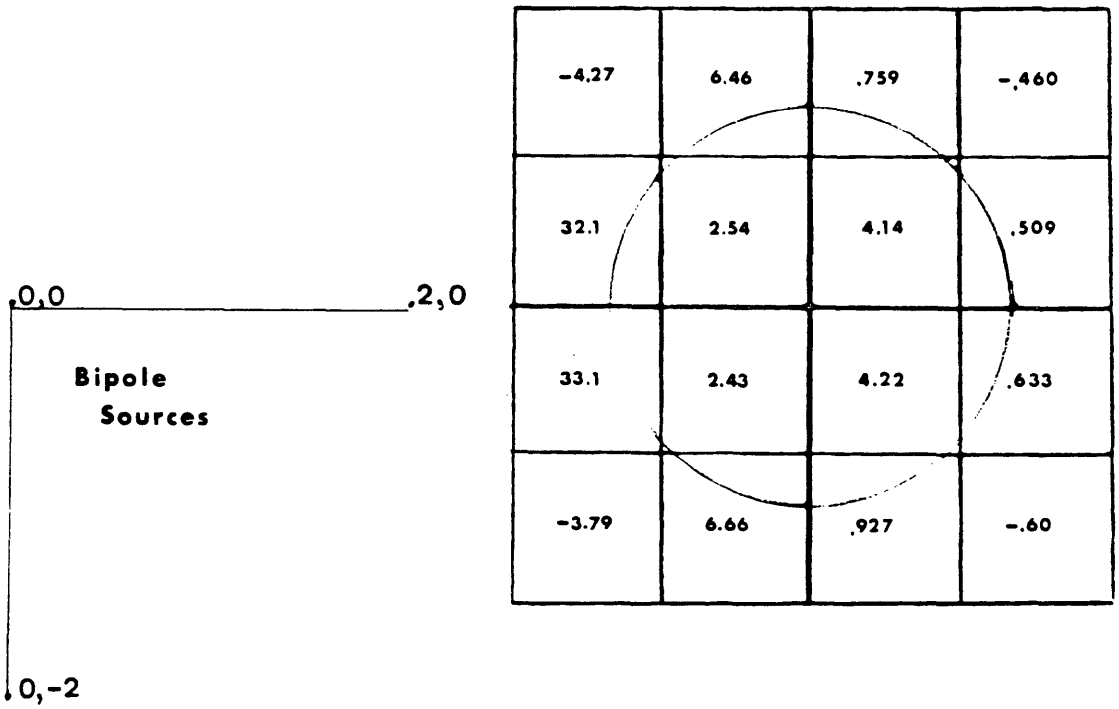

Figure 22. Inversion results from theoretical model of thin resistive layer centered at coordinates (4,0) with a radius of 1 kilometer at a depth of 1 kilometer. Transverse resistance contrast between body and overlying layers (T_2/T_1) was .3:1.

RESULTS OF INVERSION OF BELLE CREEK DATA

This same method was next applied to field data from the Belle Creek Survey. A grid was developed with a spacing of 1.5 kilometers between centers of adjacent elements, which had elements underlying observation points. Results in this case indicate that distortions of the dipole moments of the end of the east-west source were present. There were also positive dipole moments in the central portion of the map area which correlate very well with thick portions of the Muddy Sandstone. The dipoles in the northern portion of the survey area are generally negative with decreasing magnitudes away from the source. Damping factors which appeared to be best suited to this inversion were between 5×10^{-2} and 2×10^{-1}, figure 23. Slight ringing of the derived dipole values is apparent in the southern portion of the survey area with a damping of 5×10^{-2}, figure 24, while a damping of 1×10^{-1} completly removed this feature from the map, figure 26. A damping factor of 7.5×10^{-2} appears to most clearly delineate the thicker portions of the Muddy Sandstone in the area, without introducing false anomalies in the inversion results. The anomaly in the central portion of the map appeared consistently reguardless of the damping factor chosen within the optimum range. Uniform half space resistivities resulting from this analysis were

around one and the additive constants were on the order of 10^{-3}.

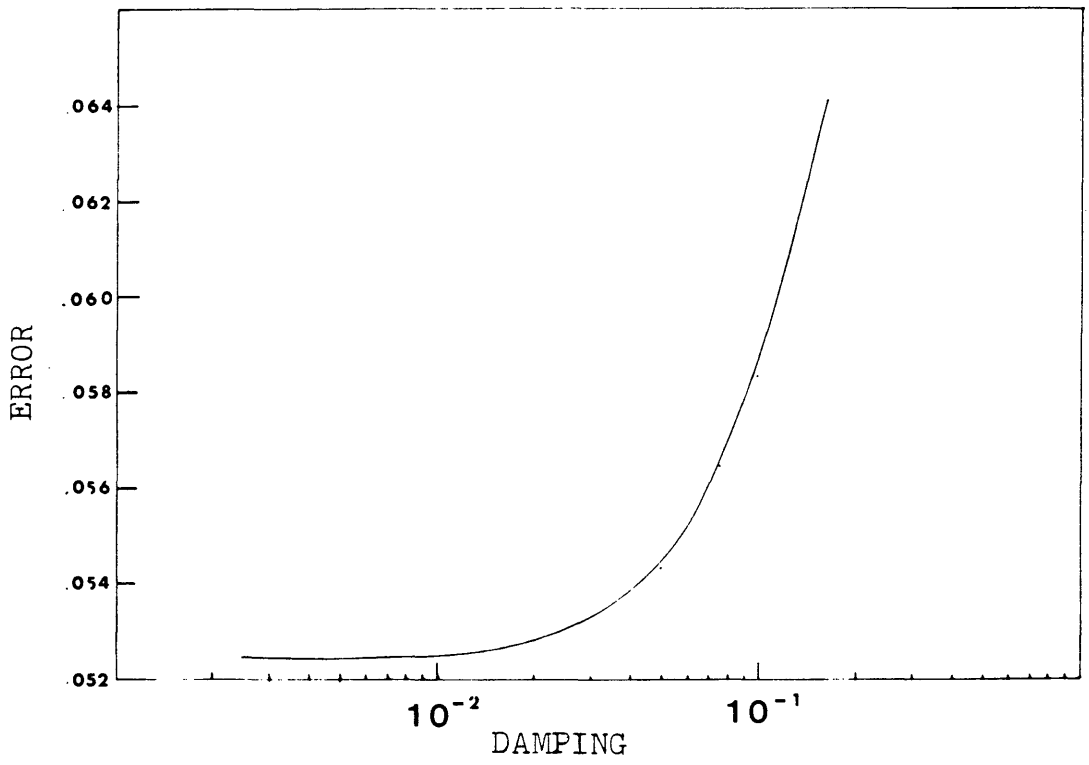

Figure 23. Error versus damping curve for inversion of Belle Creek data, with no manipulation of coefficient matrix.

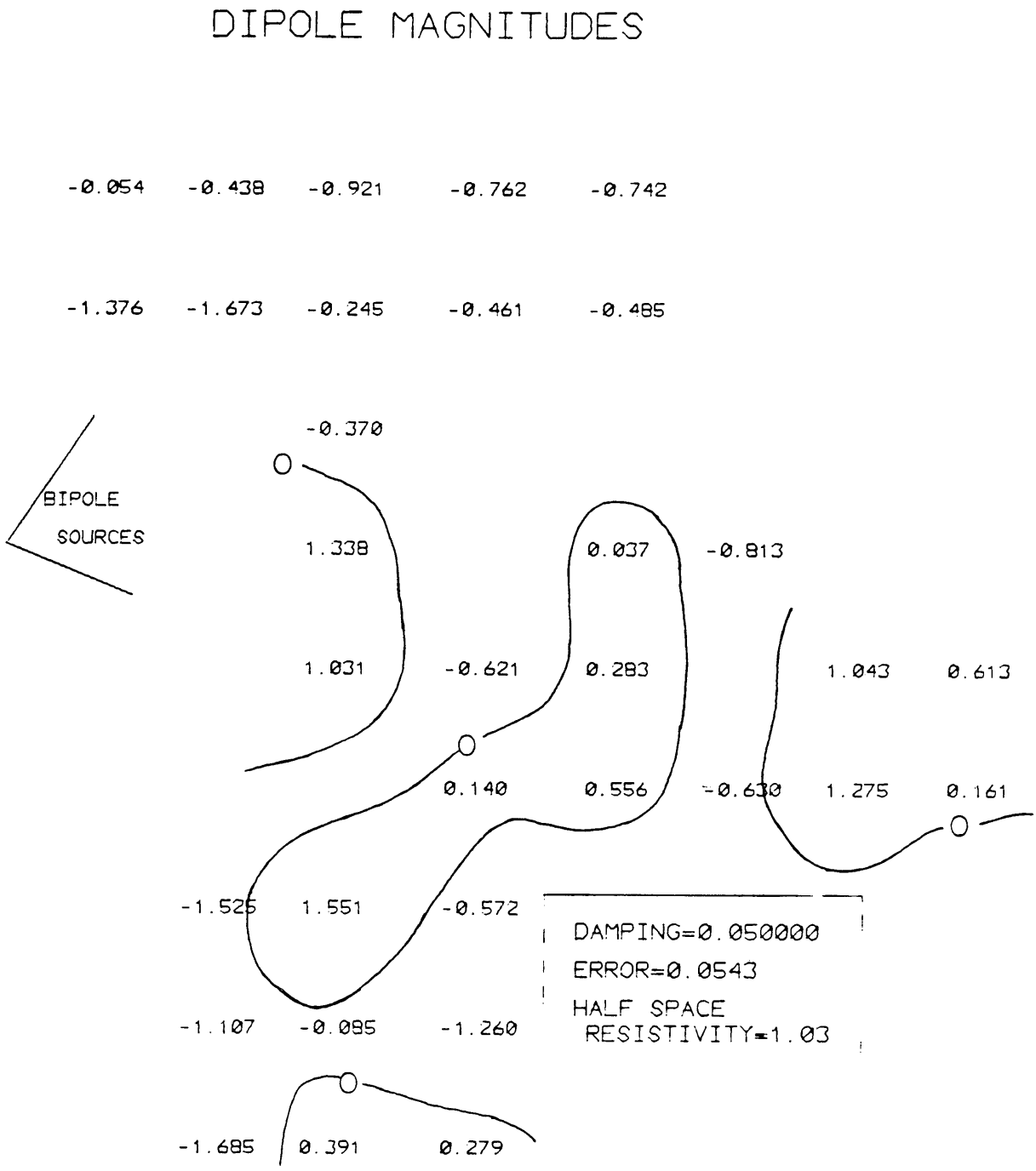

Figure 24. Dipole magnitudes from inversion of Belle Creek data, with no weighting of half space terms in **A** matrix. Underdamped.

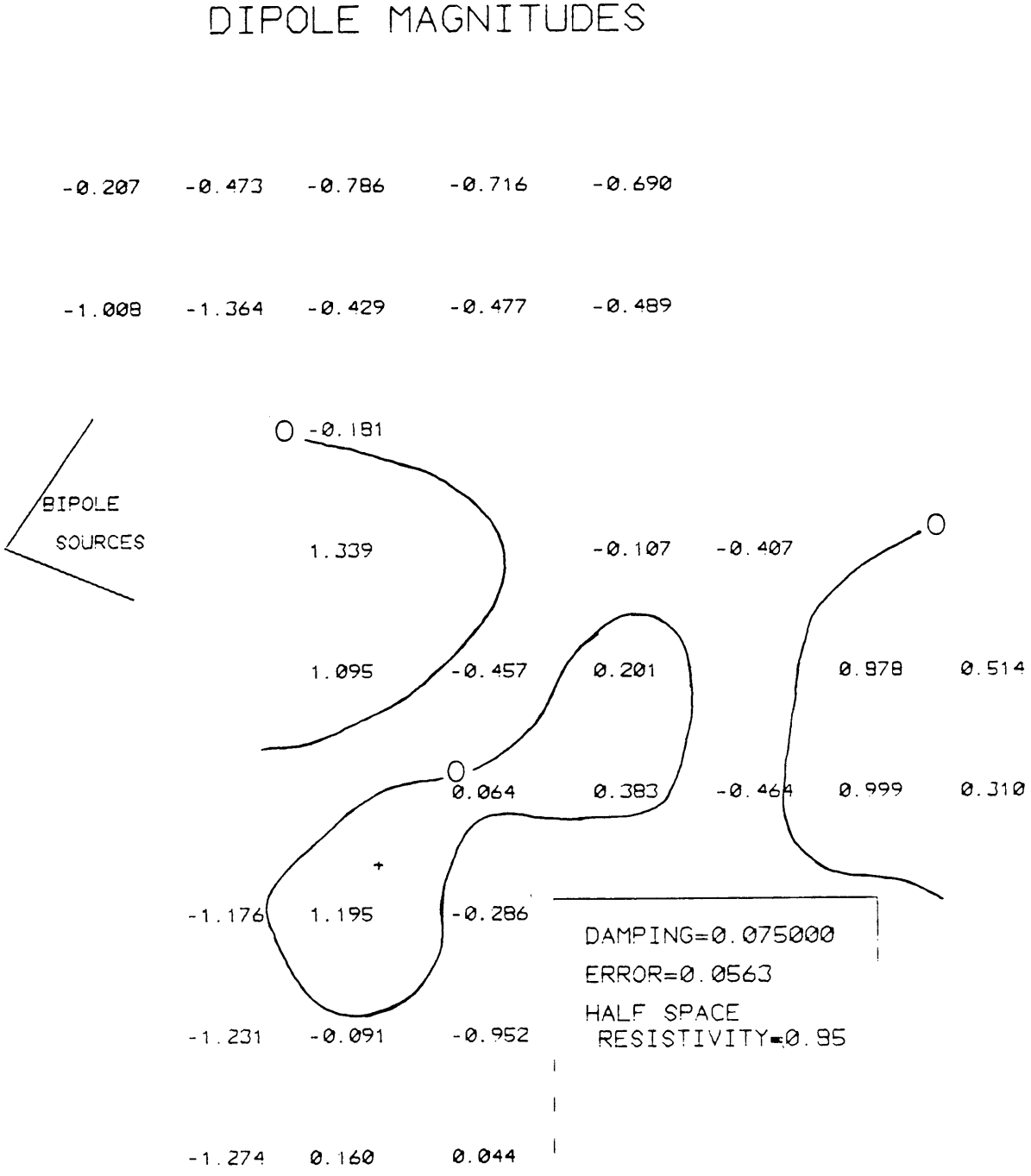

Figure 25. Dipole magnitudes from inversion of Belle Creek data, with no weighting of half space terms in A matrix. Near optimum damping.

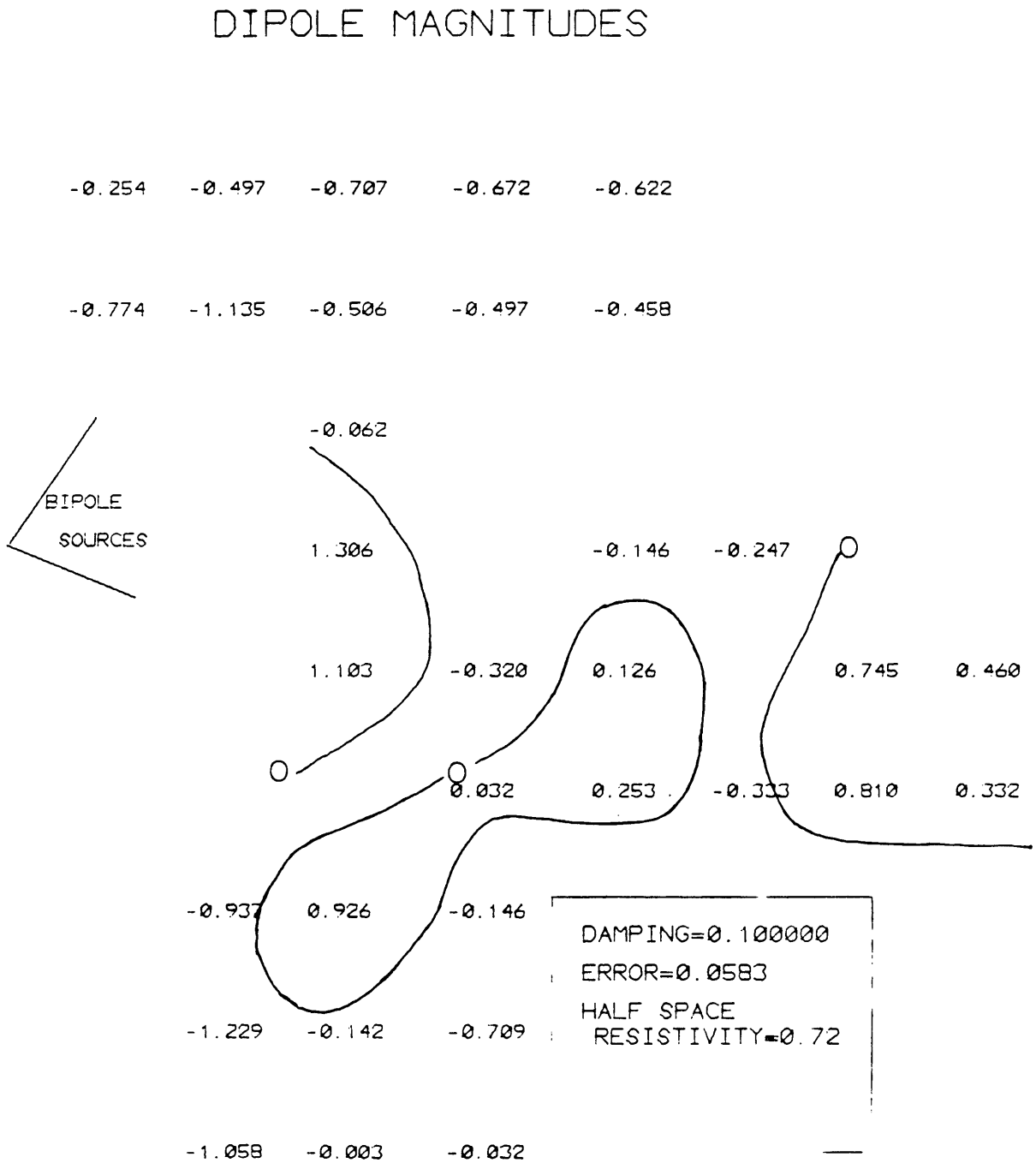

Figure 26. Dipole magnitudes from inversion of Belle Creek data, with no weighting of half space terms in A matrix. Slightly overdamped.

Several different combinations of weighting of the coefficients of the dipoles or the coefficients associated with uniform half space field or both were applied to the coefficient matrix. The main phenomena noted was that the anomalies over oil accumulations persisted and the values in the northern portion of the survey area, where there is no oil and uncomplicated geology, remained stable, negative and decreased in magnitude away from the source. Much of the oscillation of dipole moments between positive and negative values was removed by extending the grid eastward to associate it with all of the observations and removing some of the grid elements in areas where there were no measurements.

The combination which resulted in the best delineation of the thickest portions of the Muddy Sandstone and the most believable values for ρ_o, was multiplication of the uniform half space terms in the coefficient matrix by the distance between the observation point and the source. This is similar to inverting the ratio of the secondary potential (V_s) to the primary potential (V_p) due to a homogeneous half space.

Results of inversion with several damping coefficients appear in figures 28, 29, 30, and 31. The most appropriate damping in this case appears to be between 10^{-1} and 10^{-2}, figure 27.

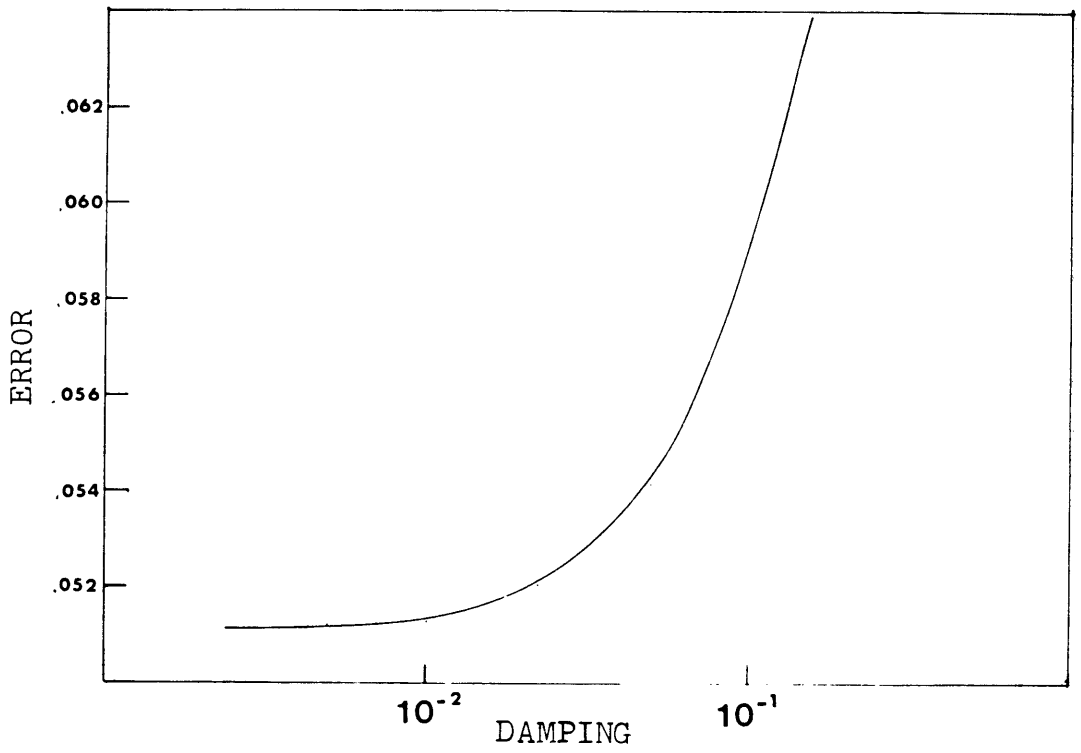

Figure 27. Error versus damping curve for final inversion of Belle Creek data, with half space terms multiplied by distance from source.

Uniform half space resistivities ranged from around 2.5 for damping factors less than 10^{-2}, to less than one for damping factors greater than 10^{-1}. The average resistivity of the overlying section was found to be approximately 6 ohm-meters from well log analysis. Positive anomalies in this case can be correlated with Muddy Sandstone thickness over 20 feet (figure 16).

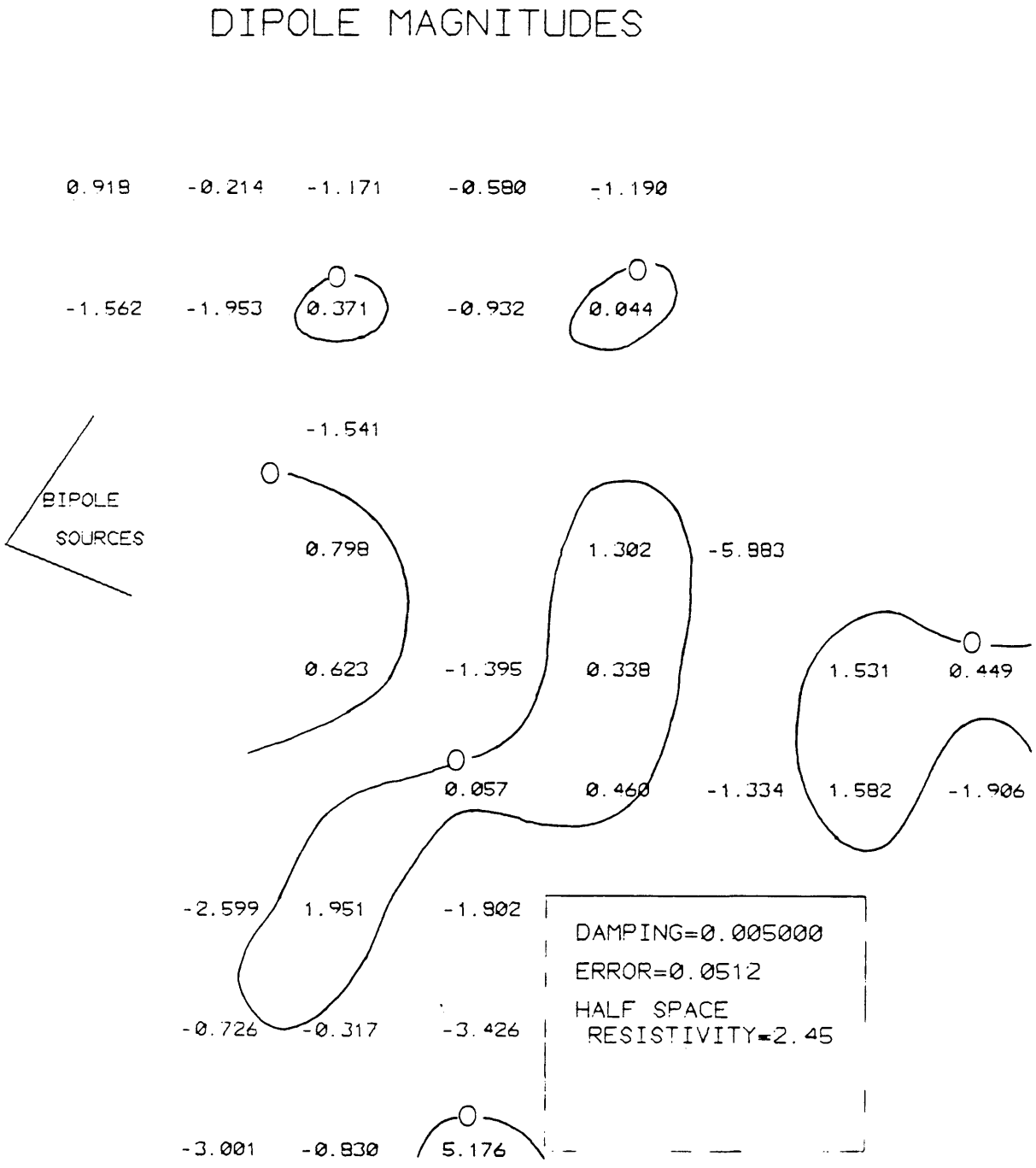

Figure 28. Dipole magnitudes from inversion of Belle Creek data, with half space terms multplied by distance from source. Underdamped.

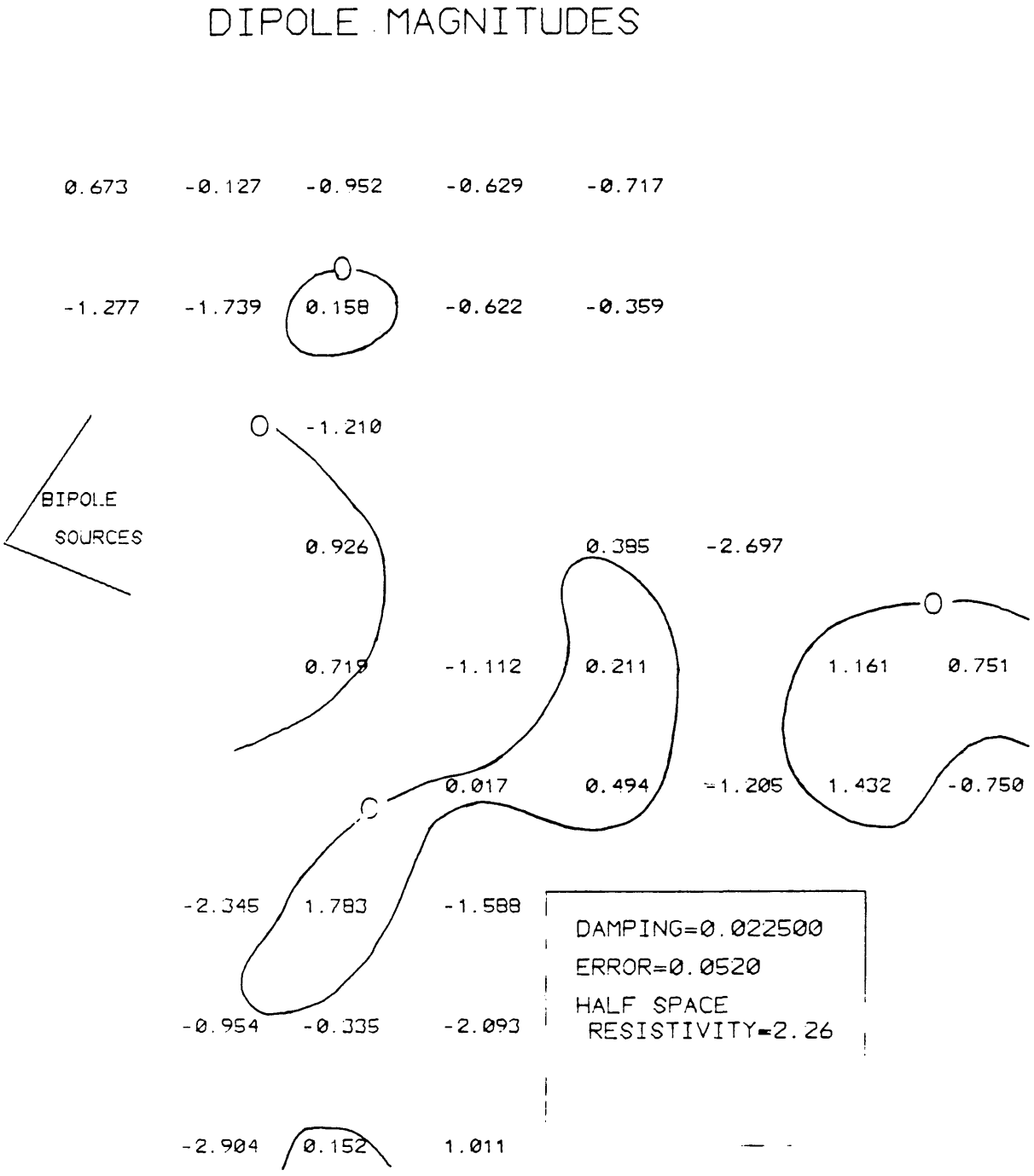

Figure 29. Dipole magnitudes form inversion of Belle Creek data, with half space terms multiplied by distance form source. Near optimum damping.

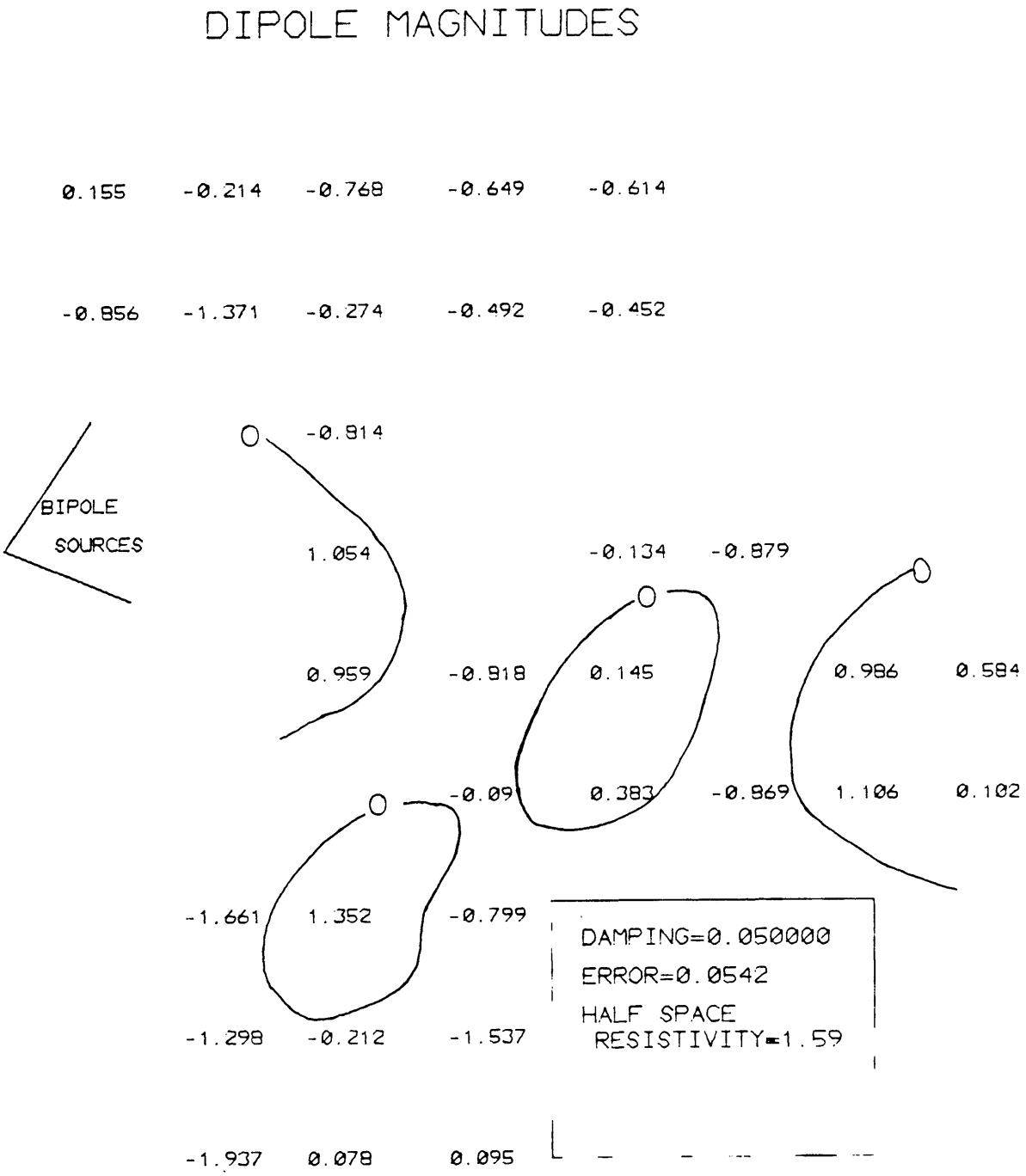

Figure 30. Dipole magnitudes from inversion of of Belle Creek data, with half space terms multiplied by distance from source. Near optimum damping.

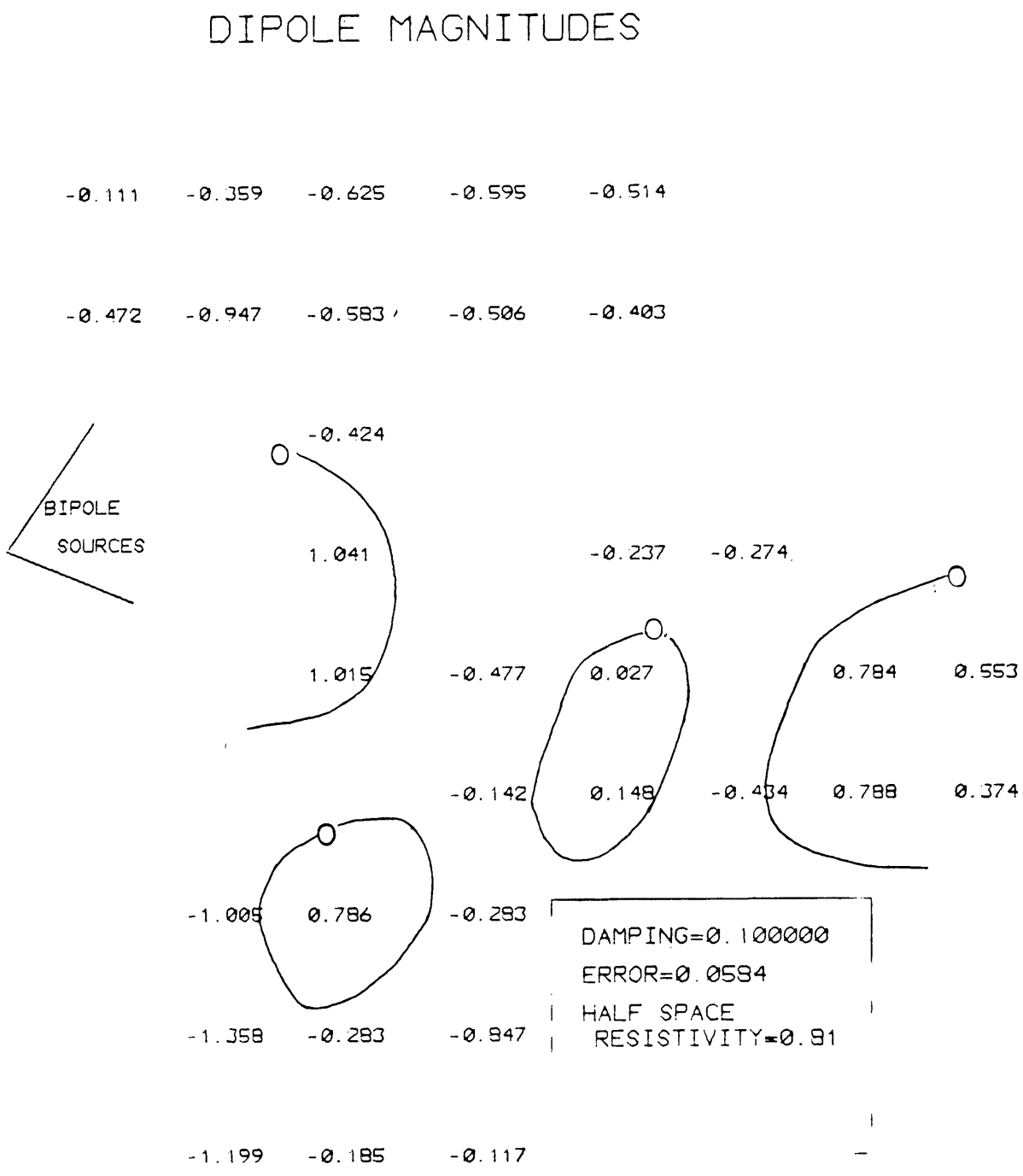

Figure 31. Dipole magnitudes from inversion of Belle Creek data, with half space terms multiplied by distance from source. Overdamped.

There was a positive anomaly which appeared in the extreme eastern portion of the survey area for both inversion procedures. This anomaly occurs in the same region where high resistivities and positive vertical derivatives occured in previous analysis of the data. This is probably due to the topography as indicated by the bipole-dipole apparent resistivity maps. There was also a relatively low signal to noise ratio in the extreme eastern portion of the survey area.

The errors described previously are generally large. Their magnitudes are near that of the smallest signals observed. The relatively large magnitude of the errors in fit to the observed data might indicate that near surface effects, causing rapid variation in potential with distance are ignored by the inversion procedure.

Results of inversion of monopole potentials at Belle Creek apparently exhibit a remarkable capacity to delineate producing zones as long as proper care is taken in choosing the proper damping factor for the inversion procedure. This fact, when coupled with the barely adequate measuring equipment and crude field procedure, indicates that the method is truly powerful in its own right.

CONCLUSION

From analysis presented in this thesis it is apparent that the bipole-dipole direct current method is able to detect anomalies in the potential field due to the presence of a thin resistive oil reservoir.

The traditional form of total field apparent resistivity calculations for the bipole-dipole mapping method was unable to delineate anomalies due to the presence of oil. This phenomena is probably due to the fact that a thin highly resistive layer of infinite extent would produce an anomaly of only one percent of the primary field for $T_1/T_2=.01$, (Keller 1968). There are disruptions of the apparent resistivities in the area of thick accumulations of the pay sand, but it would be difficult to prove that these are due to oil rather than merely noise in the data.

Second vertical derivative calculations met significantly greater success in determining areas of thicker oil accumulations. Two anomalous positive areas of the second vertical derivatives were apparent on maps of the second vertical derivative of the potential from both sources. These positive anomalies were consistently displaced away from the source by a distance of approximately the radius of the body. Theoretical models of second vertical derivatives of a thin resistive layer also exhibited closed positive anomalies which

were displaced away from the body in a direction away from the source. Determination of drilling locations on the basis of positions of these anomalies should probably be attempted only when results are used in conjunction with other types of information.

Inversion of the potential due to the bipole source was able to delineate the producing zones in their proper locations. Extreme care must be taken in selection of proper damping factors to avoid ringing in the results, caused by too little damping, or supressing anomalies which are present by overdamping the solution. In spite of the various grids and methods applied to the inversion procedure, anomalies over thicker portions of the pay zone persisted when the proper damping factor was chosen according to the sharp rise in the error curve.

Two out of three forms of analysis of the Belle Creek data appeared to detect anomalies which might be due to the presence of a thin resistive layer in the subsurface. Standard bipole-dipole apparent resistivity calcualtions were not able to delineate anomalies caused by a thin resistive layer. Second vertical derivative calculations, along with the inversion procedure appeared to consistently delineate thicker portions of the Muddy Sandstone in the producing area.

The bipole-dipole mapping method, when data are analyzed by the above methods, apparently exhibits a great potential for directly detecting oil accumulations from measurements made on the surface. The techniques described could be used in conjunction with other geophysical exploration techniques to increase the success ratio of land based exploration techniques.

APPENDIX 1

Computer file containing field data in the form used for all further calculations. It can be read in a Fortran "-G " format in the following manner: Station number, source current strength, pot location #1, potential difference #1, center pot location, potential difference #2, pot location #3, potential difference #3,pot location #4, potential difference #4. North-south source measurements are designated by positive source current strengths, and east-west source measurements are designated by negative source current strenghts.

```
1 60.0 451 -177 -1.9 528 -177 0.42 602 -215 -1.65 527 -257 2.36 529 -100
1 -87.5 451 -177 20.7 528 -177 -8.35 602 -215 -3.73 527 -257 -.36 529 -100
2 60.66 741 -293 -.50 671 -257 .348 602 -215 -1.42 652 -333 1.36 712 -188
2 -65.25 741 -293 -2.59 671 -257 3.22 602 -215 1.04 652 -333 -.46 712 -188
3 62.8 742 -292 .36 811 -330 -.26 868 -387 .805 781 -394 1.03 852 -262
3 -114.3 742 -292 -2.79 811 -330 1.59 868 -387 .607 781 -394 -.493 852 -262
4 80.0 868 -387 -.185 924 -441 .291 1003 -444 -.710 928 -360 .650 924 -517
4 -93.0 868 -387 -.923 924 -441 1.106 1003 -444 -.459 928 -360 .361 924 -517
5 59.9 1158 -444 -.30 1080 -444 .21 1003 -444 -.46 1081 -523 .484 1083 -364
5 -79.0 1158 -444 .744 1080 -444 -.503 1003 -444 -.212 1081 -523 .178 1083 -364
6 80.0 1158 -444 -.224 1238 -444 .148 1316 -444 -.437 1248 -526 .436 1239 -371
6 -96.0 1158 -444 .577 1238 -444 -.509 1316 -444 -.158 1248 -526 .171 1239 -371
7 83.0 1471 -467 .001 1393 -446 .001 1316 -444 -.226 1398 -527 .381 1405 -376
7 -98.0 1471 -467 -.272 1393 -446 .498 1316 -444 .001 1398 -527 .001 1405 -376
8 -82.0 1471 -467 .001 1543 -497 -.06 1611 -473 -.260 1527 -575 .213 1555 -409
8 47.5 1471 -467 .192 1543 -497 -.254 1611 -473 .001 1527 -575 .001 1555 -409
9 -64.0 1710 -352 .234 1660 -414 -.312 1611 -473 -.226 1722 -462 .203 1600 -365
9 49.5 1710 -352 -.130 1660 -414 .163 1611 -473 -.180 1722 -462 .263 1600 -365
10 44.1 1710 -352 .001 1788 -332 .001 1863 -310 -.185 1789 -410 .135 1787 -261
10 -108.0 1710 -352 -.296 1788 -332 .384 1863 -310 .05 1789 -410 -.03 1787 -261
13 72.0 776 -471 -.560 781 -394 .950 811 -330
13 -74.0 776 -471 -.736 781 -394 .404 811 -330
14 72.0 776 -471 .527 750 -543 -.778 697 -600 .290 812 -590 -.340 676 -519
14 -76.0 776 -471 .498 750 -543 -.420 697 -600 -.875 812 -590 1.336 676 -519
15 72.0 648 -754 -.339 664 -676 .480 697 -600 .356 744 -695 -.462 589 -662
15 -78.0 648 -754 -.770 664 -676 .893 697 -600 -.464 744 -695 .715 589 -662
16 74.0 648 -754 .197 622 -835 -.420 592 -908 .279 694 -846 -.535 550 -807
16 -80.0 648 -754 .631 622 -835 -.832 592 -908 -.183 694 -846 .248 550 -807
17 72.0 592 -908 .100 606 -986 -.060 592 -1063 .351 673 -973 -.296 536 -1002
17 -80.0 592 -908 -.378 606 -986 .599 592 -1063 .219 673 -973 -.317 536 -1002
18 73.0 592 -1063 -.077 590 -1142 .249 633 -1207 .261 658 -1107 -.269 519 -1120
18 -81.0 592 -1063 .356 590 -1142 -.184 633 -1207 .274 658 -1107 -.001 519 -1120
19 74.0 486 -1016 -.001 452 -1086 .060 417 -1153 -.383 379 -1058 .309 519 -1120
19 -85.0 486 -1016 .309 452 -1086 -.565 417 -1153 -.213 379 -1058 .086 519 -1120
20 75.0 314 -955 -.158 305 -1033 .101 268 -1101 .364 254 -983 -.365 379 -1058
20 -86.0 314 -955 .348 305 -1033 -.652 268 -1101 .323 254 -983 -.143 379 -1058
21 72.0 254 -983 .123 233 -1053 -.246 179 -1066
21 -80.0 254 -983 .376 233 -1053 -.432 178 -1066
22 73.0 602 -215 -1.306 592 -132 2.108 558 -61
22 -83.0 602 -215 -1.303 592 -132 2.623 558 -61
23 73.0 510 84 3.514 536 11 -3.395 558 -61 2.234 461 23 -.442 616 23
23 -84.5 510 84 -3.136 536 11 1.21 558 -61. 5.538 461 23 -5.725 616 23
24 66.0 496 248 3.485 498 166 -4.840 510 84 -2.883 421 166 6.097 580 166
24 -73.0 496 248 -3.347 499 166 5.317 510 84 -1.489 421 166 1.387 580 166
25 72.0 496 248 .364 511 325 -1.264 518 389 -4.70 437 304 8.930 587 343
25 -80.0 496 248 2.832 511 325 -2.252 518 389 1.437 437 304 -1.878 587 343
26 70.0 379 460 3.853 449 426 -4.580 518 389 -3.809 451 503 3.717 451 344
26 -80.0 379 460 -2.149 449 426 2.284 518 389 -1.031 451 503 1.903 451 344
27 68.0 379 460 -8.138 300 457 5.693 221 455 -1.009 300 537 2.121 300 376
27 -81.0 379 460 2.170 300 457 -3.104 221 455 -3.817 300 537 .969 300 376
28 70.0 217 607 -6.159 201 531 1.021 221 455 -5.182 123 536 2.656 281 527
28 -79.0 217 607 .535 201 531 .734 221 455 -1.423 123 536 2.011 281 527
29 69.0 217 607 3.401 239 680 1.004 314 653
29 -79.0 217 607 -.663 239 680 1.497 314 653
30 69.0 441 717 -.989 368 700 2.783 314 653 -1.606 342 770 1.527 413 632
30 -80.0 441 717 .977 368 700 -.859 314 653 -.543 342 770 .870 413 632
```

31 70.0 441 717 -.125 514 685 .483 568 633 -1.350 568 739 1.995 459 629
31 -80.5 441 717 .944 514 685 -1.137 568 633 .380 568 739 -.474 459 629
32 70.0 568 633 -1.082 651 624 1.503 716 599 .626 660 545 -.635 675 700
32 -81.0 568 633 .908 651 624 -.769 716 599 .928 660 545 -.749 675 700
33 70.0 858 523 1.137 794 569 -.815 716 599 .565 755 501 -.471 824 637
33 -81.0 858 523 -.783 794 569 .776 716 599 .609 755 501 -.373 824 637
34 70.0 858 523 -.652 930 544 .842 1003 560
34 -81.0 858 523 -.048 930 544 .075 1003 560
35 70.0 1003 560 .472 1064 611 9999 1124 570 -.501 1138 620 .234 1040 679
35 -82.0 1003 560 .316 1064 611 9999 1124 570 .001 1138 620 -.508 1040 679
36 68.0 1158 -444 -.629 1186 -369 .495 1188 -286 -.141 1259 -400 .001 1115 -340
36 -79.0 1158 -444 .001 1186 -369 .001 1188 -286 -.447 1259 -400 .520 1115 -340
37 68.0 1186 -286 -.393 1171 -209 .450 1175 -150 .842 1251 -211 -.191 1096 -237
37 -80.0 1186 -286 .084 1171 -209 -.087 1175 -150 -.408 1251 -211 .464 1096 -237
38 68.0 1174 -13 .516 1145 -82 -.665 1175 -150 .093 1225 -72 -.183 1073 -115
38 -82.0 1174 -13 -.460 1145 -82 .196 1175 -150 -.504 1225 -72 .674 1073 -115
39 79.0 481 -722 .431 496 -755 -.206 550 -807
39 -92.0 481 -722 -.606 496 -755 .507 550 -807
40 79.0 481 -722 -1.094 402 -712 .963 324 -694 .207 402 -792 -.213 395 -632
40 -93.0 481 -722 -.522 402 -712 .469 324 -694 -1.250 402 -792 1.984 395 -632
41 81.0 738 -945 .320 679 -890 -.205 622 -835
41 -96.0 738 -945 -.436 679 -890 .672 622 -835
42 82.0 679 -890 -.264 738 -945 .137 785 -1008 -.189 673 -981 .303 809 -914
42 -96.0 679 -890 .433 738 -945 -.509 785 -1008 -.506 673 -981 .438 809 -914

APPENDIX 2

Computer program which was used to calculate and plot apparent resistivities and second vertical derivatives from bipole-dipole measurements made in Belle Creek, Montana. This program uses the data described in appendix 1.

```
      LOGICAL LPOS,ROAP,DRIV
        DIMENSION X(5),Y(5),V(4),FACT(4),RHOA(4),XS(2),YS(2)
      DIMENSION DIS(4),E(4),ET(4),EY(4),CS(4),SN(4),DSQ(5)
      DIMENSION XR(4),YR(4),XSF(2),YSF(2)
      DIMENSION DIST(4)
      DIMENSION LITR(6),LITD(7)
      COMMON/SLOC/XS,YS,IS
      DATA LITR / 'APPAR','ENT R', 'ESIST','IVITY',' FROM',' ET  '/
      DATA LITD/'SECON','D VER','TICAL',' DERI','VATIV','ES OF',' POT '/
      DATA FACT/ .962, 1.034, 1.005, 1.043/
      FCTR=.630
 1004   FORMAT('ENTER PLOT TYPE(1=RHOA,2=DERIV); ',$)
 1005   FORMAT(10G)
      WRITE(4,1004)
      READ(4,1005)IFPLOT
      ROAP=IFPLOT.EQ.1
      DRIV=IFPLOT.EQ.2
      XS(1)=174./162.
      YS(1)=259./162.
      XS(2)=254./162.
      YS(2)=-104./162.
      LPOS=.TRUE.
      JPLOT=0
      IF(ROAP.OR.DRIV)JPLOT=IPLOT(-10)
      IP=NEWPEN(2)
      IF(JPLOT.NE.0)STOP 'PLOT FILE'
      CALL PLOT(1.,5.9,-3)
   1    READ(1,1000,END=100)N,AMP,X(1),Y(1),V(1),X(2),Y(2),V(2)
     2,X(3),Y(3),V(3),X(4),Y(4),V(4),X(5),Y(5)
      IF(.NOT.LPOS.AND.AMP.GT.0.) GO TO 1
      IF(LPOS.AND.AMP.LT.0.)GO TO 1
 1000  FORMAT (20G)
C       CHANGES DISTANCES TO KILOMETERS
      DO 10 J=1,5
      X(J)=X(J)/162.
      Y(J)=Y(J)/162.
  10    CONTINUE
      DO 2 N=1,2
      XSF(N)=XS(N)*FCTR
      YSF(N)=YS(N)*FCTR
   2    CONTINUE
      IS=1
      IF(AMP.LT.0.0)IS=2
      IF(N.GT.1) GO TO 3
      IF(ROAP) CALL SYMBOL(.8,4.05,.2,20HAPPARENT RESISTIVITY,0.0,20)
      IF (DRIV) CALL SYMBOL(.8,4.05,.2,20HVERTICAL DERIVATIVES,0.0,20)
        CALL PLOT(0.,0.,3)
      CALL PLOT (XSF(IS),YSF(IS),2)
   3    CONTINUE
C     NORMALIZES VOLTAGES TO CURRENTS AND EACH OTHER
      DO 7 L=1,5
```

```
        K1=L
      L1=L
      IF(L.EQ.2)GO TO 7
        IF(L.GT.2)K1=K1-1
      DIS(K1)=DST(L1,X,Y)
    7   CONTINUE
      DO 20 I=1,4
      V(I)=FACT(I)*V(I)/ABS(AMP)
      E(I)=V(I)/DIS(I)
   20   CONTINUE
C     CALL PRINT (E,4,'E')
C  CALCULATES APPARENT RESISTIVITIES IN MEASURED DIRECTIONS
      IF(E(3).EQ.0.0) GO TO 1
      CALL RHOAP(X,Y,E,RHOA,D2UDZ2)
      IF(ROAP)CALL PLOTRA(X,Y,RHOA,N,FCTR)
      DRV=D2UDZ2
      IF(DRIV)CALLPLOTDR(X,Y,N,DRV,FCTR)
      WRITE(6,1001)N,AMP
 1001   FORMAT(1H ,3X,'STAION: ',I3,/3X,'CURRENT: ',F7.2)
      WRITE(6,1002)
 1002   FORMAT(1H ,6X,'X',15X,'Y',15X,'V',10X,'RHOA',10X,'DERIV')
      WRITE(6,1003)X(2),Y(2),X(1),Y(1),V(1),RHOA(1),D2UDZ2,X(3),Y(3)
     2,V(2),RHOA(2),X(4),Y(4),V(3),RHOA(3),X(5),Y(5),V(4),RHOA(4)
      WRITE(10,999)X(2),Y(2),DRV
  999   FORMAT(1H ,3G)
 1003   FORMAT(1H ,2G/5G/4G/4G/4G)
      GO TO 1
      IB=ISETAB(2)
  100   AMP=0.0
      CALL PLOT(0.0,0.0,999)
        IF(.NOT.LPOS)GO TO 200
      JPLOT=0
      IF(ROAP.OR.DRIV)JPLOT=IPLOT(-10)
      IP=NEWPEN(2)
      IF (JPLOT.NE.0)STOP 'PLOT FILE'
      CALL PLOT(1.,5.9,-3)
      LPOS=.FALSE.
      REWIND 1
      GO TO 1
      CALL PLOT(0.0,0.0,999)
  200   STOP
      END
```

```
      SUBROUTINE RHOAP(X,Y,E,RHOA,D2UDZ2)
      DIMENSION XT(5),YT(5),ET(4)
      DIMENSION E(4),RHOA(4),X(5),Y(5),XST(2),YST(2)
      COMMON/SLOC/XS(2),YS(2),IS
      CALL TRSLT(5,X,Y,XT,YT)
      CALL ETL(XT,YT,E,ET,D2UDZ2)
      XST(1)=-X(2)
      XST(2)=XS(IS)-X(2)
      YST(1)=-Y(2)
      YST(2)=YS(IS)-Y(2)
      XA=-XST(1)
      YA=-YST(1)
      XB=-XST(2)
      YB=-YST(2)
      XA2=XA*XA
      YA2=YA*YA
      XB2=XB*XB
      YB2=YB*YB
      AO=SQRT(YA2+XA2)
      BO=SQRT(YB2+XB2)
      AO3=AO*AO*AO
      BO3=BO*BO*BO
      DUM1=(YA/AO3)-(YB/BO3)
      DUM2=(XA/AO3)-(XB/BO3)
      DUM3=DUM1*DUM1
      DUM4=DUM2*DUM2
      DEN=SQRT(DUM3+DUM4)
      DNO=6.283185307/DEN
      DO 9 K=1,4
      RHOA(K)=DNO*ET(K)
    9   CONTINUE
      RETURN
      END
```

```
      SUBROUTINE TRSLT(N,X,Y,XT,YT)
      DIMENSION X(1),Y(1),XT(1),YT(1)
      DO 1 I=1,N
      XT(I)=X(I)-X(2)
      YT(I)=Y(I)-Y(2)
    1   CONTINUE
      RETURN
      END
```

```
      FUNCTION DST(K,X,Y)
      DIMENSION X(1),Y(1)
      XD=X(K)-X(2)
      YD=Y(K)-Y(2)
      X2=XD*XD
      Y2=YD*YD
      DST=SQRT(X2+Y2)
      RETURN
      END
```

```
      SUBROUTINE ETL(XT,YT,E,ET,D2UDZ2)
      DIMENSION XT(5),YT(5),E(4),ET(4),EY(4),CS(4),SN(4),DSQ(5)
      DO 1 I=1,4
      K=I
      IF(I.GT.1)K=I+1
      DSQ(K)=XT(K)*XT(K)+YT(K)*YT(K)
    1   CONTINUE
      M=4
      N=3
      DO 2 J=1,2
      CS(J)=(XT(1)*XT(M)+YT(1)*YT(M))/SQRT(DSQ(1)*DSQ(M))
      SN(J)=SQRT(1.-CS(J)*CS(J))
      EY(J)=(E(N)-E(1)*CS(J))/SN(J)
      ET(J)=SQRT(E(1)*E(1)+EY(J)*EY(J))
      M=M+1
      N=N+1
    2   CONTINUE
      M1=5
      N1=4
      DO 3  L=3,4
      CS(L)=(XT(3)*XT(M1)+YT(3)*YT(M1))/SQRT(DSQ(3)*DSQ(M1))
      SN(L)=SQRT(1.-CS(L)*CS(L))
      EY(L)=(E(N1)-E(2)*CS(L))/SN(L)
      ET(L)=SQRT(E(2)*E(2)+EY(L)*EY(L))
      M1=M1-1
      N1=N1-1
    3   CONTINUE
      D2UDZ2=DEDZ(CS,SN,DSQ,E,EY)
      RETURN
      END
```

```
      FUNCTION DEDZ(CS,SN,DSQ,E,EY)
      DIMENSION E(4),EY(4),THETA(4),DIST(4),DSQ(5),CS(4),SN(4)
      DO 1I=1,4
      THETA(I)=ACOS(CS(I))
      DIST(I)=SQRT(DSQ(I))
    1   CONTINUE
C   CALCULATES Y DISTANCES
      DY1=ABS(DIST(3)*SN(1))
      DY2=ABS(DIST(3)*SN(1))+ABS(DIST(2)*SIN(THETA(1)+THETA(4)))
      ADY1=(DY1+DY2)/2.
      DY3=ABS(DIST(4)*SN(2))
      DY4=ABS(DIST(4)*SN(1))+ABS(DIST(2)*SIN(THETA(2)+THETA(3)))
      ADY2=(DY3+DY4)/2.
      ADY=(ADY1+ADY2)/2.
C   CALCILATES X DISTANCES
      ADX1=DIST(1)
      DX3=ABS(DIST(2)*COS(THETA(1)+THETA(4)))+ABS(DIST(4)*CS(2))
      DX4=ABS(DIST(2)*COS(THETA(2)+THETA(3)))+ABS(DIST(3)*CS(1))
      ADX2=(DX3+DX4)/2.
      ADX=(ADX1+ADX2)/2.
C    ROTATES E-FIELD TO PREPENDICULAR AND FINDS DERIVATIVES
      ROT1=(3.141592654-(THETA(1)+THETA(4)))
      ROT2=-(3.141592654-(THETA(2)+THETA(4)))
      AEY1=(EY(1)+EY(4)*COS(ROT1))/2.
      AEY2=(EY(2)+EY(3)*COS(ROT2))/2.
      DEDY=(AEY2+AEY1)/ADY
      EX1=E1
      EX2=(E(3)*COS(ROT2)+E(4)*COS(ROT1))/2.
      DEDX=(EX1+EX2)/2.
      DEDZ=-(DEDX+DEDY)
C     CALL PRINT(DEDZ,1,'DEDZ')
      RETURN
      END
```

```
      SUBROUTINE PRINT(X,N,TAG)
      DIMENSION X(N)
      WRITE(4,1000)TAG,X
 1000    FORMAT(1HO,A5,(5(1PE11.2)))
      RETURN
      END
```

```
      SUBROUTINE PLOTRA(X,Y,RHOA,N,FCTR)
      DIMENSION X(5),Y(5),RHOA(4),XR(4),YR(4)
      IF(N.EQ.35) RETURN
      DO 1 I=1,5
      X(I)=X(I)*FCTR
      Y(I)=Y(I)*FCTR
    1   CONTINUE
      CALL PLOT(X(2),Y(2),3)
      DO 2 J=1,5
C     IF (J.EQ.2)GO TO 2
      CALL PLOT(X(J),Y(J),2)
      CALL PLOT(X(2),Y(2),3)
    2   CONTINUE
      XR(1)=(X(1)-X(4))*.5+X(2)
      YR(1)=(Y(1)-Y(4))*.5+Y(2)
      XR(2)=(X(1)-X(5))*.5+X(2)
      YR(2)=(Y(1)-Y(5))*.5+Y(2)
      XR(3)=(X(3)-X(5))*.5+X(2)
      YR(3)=(Y(3)-Y(5))*.5+Y(2)
      XR(4)=(X(3)-X(4))*.5+X(2)
      YR(4)=(Y(3)-Y(4))*.5+Y(2)
      DO 3 K=1,4
      CALL NUMBER(XR(K),YR(K),.05,RHOA(K),0.0,2)
    3   CONTINUE
      RETURN
      END
```

```
      SUBROUTINE PLOTDR(X,Y,N,D2UDZ2,FCTR)
      DIMENSION X(5),Y(5)
      IF(N.EQ.35) RETURN
      DO 1 I=1,5
      X(I)=X(I)*FCTR
      Y(I)=Y(I)*FCTR
1     CONTINUE
      CALL PLOT (X(2),Y(2),3)
      DO 2 J=1,5
      IF (J.EQ.2) GO TO 2
      CALL PLOT(X(J),Y(J),2)
      CALL PLOT(X(2),Y(2),3)
2     CONTINUE
      XP=X(2)+.15
      YP=Y(2)+.15
      CALL NUMBER(XP,YP,.07,D2UDZ2,0.0,4)
      RETURN
      END
```

APPENDIX 3

Computer program which was used for inversion of monopole potentials to causitive dipole moments on an imaginary grid at a given depth below the surface. Input for this program is from a file created by summing connected potentials, programed by Stoyer (1979) Data are again read in in a " .G " format.

```
C THIS  IS AN INVERSION PROGRAM
      PARAMETER KAM=7300,KV=148
      DIMENSION A(KAM),X(KV),Y(KV),V(KV),P(75)
      DIMENSION AM(KAM),VM(KAM),S(160)
      DIMENSION VSTAR(160),PSTAR(160)
      DIMENSION VN(KV),PTRUE(KV),V1(KV),V2(KV)
      COMMON/DIPLS/MYE,NXE,X0,Y0,Z0
      COMMON /SOURC/ XS1,YS1,XS2,YS2,X21,Y21,X22,Y22
      COMMON /GRID/ NGD,XG(50),YG(50)
      WRITE(4,1414)
 1414 FORMAT(' XS1,YS1,XS2,YS2:')
      READ(4,901) XS1,YS1,XS2,YS2
      WRITE(6,1414)
      WRITE(6,901) XS1,YS1,XS2,YS2
      X21=XS1*XS1
      Y21=YS1*YS1
      X22=XS2*XS2
      Y22=YS2*YS2
      GO TO 50
      SCALE=1.E-4
      WRITE(4,500)
  500   FORMAT(1H ,'PICK A NUMBER')
      READ(4,501) NUMB
  501   FORMAT(4G)
      CALL SETRAN(NUMB)
      WRITE(4,900)
  900   FORMAT(1H ,'INPUT NOBS,MYE,NXE')
      READ(4,901)NOBS,MYE,NXE
  901   FORMAT(10G)
      READ (11,1000)(X(I),Y(I),I=1,NOBS)
 1000   FORMAT(2G)
      NP=NGD
      IF(NOBS.GT.KV)STOP'NOBS'
      IF(NP.GT.50)STOP'NP'
      IF(NOBS*(NP+3).GT.KAM)STOP'NOBS*NP'
CNP=(MYE-1)*(NXE-1)
      NXE=10
      MYE=NP/NXE +1
      READ(12,1002)(P(K),K=1,NP)
 1002   FORMAT(4G)
      WRITE(6,1030)
 1030   FORMAT(1H ,'REAL P VALUES')
      CALL PRNT(6,P,NP)
      CALL SWITCH(P,PTRUE,NP,1)
   50   OPEN(UNIT=2,FILE='VOLTS')
      OPEN(UNIT=3,FILE='GRID')
      DO55I=1,50
      READ(3,503,END=56) XG(I),YG(I)
      NGD=I
   55 CONTINUE
   56 CONTINUE
```

```
      READ (2) NOBS,(X(I),I=1,NOBS),(Y(I),I=1,NOBS),
     1(V1(I),I=1,NOBS)
      READ(2) NOBS,(X(I),I=1,NOBS),(Y(I),I=1,NOBS),
     1(V2(I),I=1,NOBS)
      WRITE(4,502)
 502    FORMAT(1H ,'INPUTMYE,NXE,DX,DY,X0,Y0,Z0')
      READ(4,503) MYE,NXE,DX,DY,X0,Y0,Z0
 503    FORMAT(10G)
C     NP=(NXE-1)*(MYE-1)
      NP=NGD
      CALL GENRAT(X,Y,DX,DY,NOBS,NP,A,V,V1,V2)
      WRITE(6,502)
      WRITE(6,503) MYE,NXE,DX,DY,X0,Y0,Z0
      WRITE(6,1013)
 1013   FORMAT(1H ,'ORIGINAL A MATRIX')
      CALL PRNTM(6,A,NOBS,NP)
C     CALL MULT(A,PTRUE,NOBS,NP,V)
      WRITE(6,1001)(X(J),Y(J),V(J),J=1,NOBS)
 1001   FORMAT(1H ,3G)
C     CALL ADNOIS(V,NOBS,SCALE)
C     WRITE(6,1014)
 1014    FORMAT(1H ,'VOLTAGE PLUS NOISE')
      WRITE (6,1003)(V(IN),IN=1,NOBS)
 1003   FORMAT(1H ,G)
      CALL SWITCH(A,AM,NOBS,NP)
      WRITE(6,1031)

 1031   FORMAT(1H ,' A MATRIX AFTER SWITCH')
      CALL HYSVD(A,S,VM,NOBS,NP,0,.TRUE.,.TRUE.)
      WRITE(6,1004)
      WRITE(4,1004)
 1004   FORMAT(1H ,'SINGULAR VALUES')
      CALL PRNT(6,S,NP)
      CALLPRNT(4,S,NP)
      NE=NP
C     WRITE(6,1005)
 1005   FORMAT(1H ,'U MATRIX')
C     CALL PRNTM(6,A,NOBS,NP)
C     WRITE(6,1006)
 1006   FORMAT(1H ,'V MATRIX')
C     CALL PRNTM(6,VM,NP,NP)
C CALCULATE VSTAR,WHICH IS=UTRANSPOSE*V
      CALL VSTR(A,V,NOBS,NP,VSTAR)
C PRINT VSTAR WHICH WILL BE AVECTOR OF LENGTH NOBS
      WRITE(6,1007)
 1007   FORMAT(1H ,'VSTAR ')
      CALL PRNT(6,VSTAR,NE)
  100 WRITE(4,1008)
 1008   FORMAT(1H ,'CHOOSE D SO THAT 10E-06<D/S<10E-01')
      READ(4,1009)   D
      IF(D.LT.0.)STOP
```

```
 1009   FORMAT(10G)
      CALL PSTR(D,S,VSTAR,PSTAR,NE)
      WRITE(6,1010)
 1010   FORMAT(1H ,'PSTAR VECTOR OF LENGTH  NE')
      CALL PRNT(6,PSTAR,NE)
C CALCULATE  DIPOLES BY MULT'ING PSTAR WITH V MATRIX
      CALL MULT(VM,PSTAR,NE,NP,P)

      WRITE(6,1011)
 1011    FORMAT(1H ,'DIPOLE VALUES FOR THIS D')
CCALL PRNT(6,P,NE)
      CALL PRNTM(6,P,MYE+1,NXE-1)
      CALL MULT(AM,P,NOBS,NE,VN)
      WRITE (6,1020)
 1020   FORMAT(1H ,'NEW V CALCULATED BY  P VALUES')
      CALL PRNT(6,VN,NOBS)
C        CALCULATE ERROR BETWEEN V AND VNEW
      ERV= ER1(VN,V,NOBS)
      ERP=ER1(P,PTRUE,NP)
      WRITE(6,1022) ERV,ERP,S(1),D
      WRITE(4,1022) ERV,ERP,S(1),D
1022   FORMAT(1H ,'ERV= ' ,G,'ERP= ',G,'S MAX= ',G,'DAMPING= ',G)
      WRITE(4,101)
  101   FORMAT(1H ,'DO YOU WANT THIS PLOTTED?1=YES,2=NO')
      READ(4,1009)IFPLOT
      IF(IFPLOT.EQ.2)GO TO 107
      CALL PLOTIT(P,D,ERV)
  107   CONTINUE
      GO TO 100
      END
```

```
C SUBROUTINE TO PLOT DIPOLE VALUES IN THEIR PROPER POSITIONS
      SUBROUTINE  PLOTIT(P,D,ERV)
      DIMENSION  XGP(50),YGP(50),P(1),XSP(2),YSP(2)
      COMMON/SOURC/XS1,YS1,XS2,YS2,X21,Y21,X22,Y22
      COMMON/GRID/NGD,XG(50),YG(50)
      FCTR=.630
      K=IPLOT(-2)
      IF(K.NE.0)STOP'PLOT FILE'
      IP=NEWPEN(2)
      CALL PLOT(1.,5.9,-3)
      XSP(1)=XS1*FCTR
      XSP(2)=XS2*FCTR
      YSP(1)=YS1*FCTR
      YSP(2)=YS2*FCTR
      DO 8 I=1,2
      CALL PLOT(XSP(I),YSP(I),2)
      CALL PLOT(0.,0.,3)
  8     CONTINUE
      CALL SYMBOL(.3,.3,.1,6HBIPOLE,0.0,6)
      CALL SYMBOL(.4,0.,.1,7HSOURCES,0.0,7)
      DO 9 J=1,NGD
      XGP(J)=XG(J)*FCTR
      YGP(J)=YG(J)*FCTR
      CALL NUMBER(XGP(J),YGP(J),0.1,P(J),0.0,3)
  9     CONTINUE
C     GO TO 18
      CALL SYMBOL(4.5,-3.10,.12,8HDAMPING=,0.0,8)
      CALL NUMBER(5.47,-3.1,.12,D,0.0,6)
      CALL SYMBOL(4.5,-3.4,.12,6HERROR=,0.0,6)
      CALL NUMBER(5.227,-3.4,.12,ERV,0.0,4)
      CALL SYMBOL(4.5,-3.7,.12,10HHALF SPACE,0.0,10)
      CALL SYMBOL(4.6,-3.9,.12,12HRESISTIVITY=,0.0,12)
      CALL NUMBER(5.92,-3.9,.12,P(NGD+3),0.0,2)
      CALL PLOT(4.25,-2.75,3)
      CALL PLOT(6.75,-2.75,2)
      CALL PLOT(6.75,-4.75,2)
      CALL PLOT(4.25,-4.75,2)
      CALL PLOT(4.25,-2.75,2)
      CALL SYMBOL(1.6,4.0,.2,17HDIPOLE MAGNITUDES,0.0,17)
      CALL PLOT(0.,0.,999)
  18    CONTINUE
      RETURN
      END
```

```
      SUBROUTINE GENRAT(X,Y,DX,DY,NOBS,NP,A,V,V1,V2)
      DIMENSION A(1),X(1),Y(1),V(1),V1(1),V2(1)
      IJ=1
      DO 100 I=1,NOBS
      CALL ROWFIL(A(IJ),X(I),Y(I),DX,DY,NP)
      IJ=IJ+NP
      CALL FOLSOR(A(IJ),V(I),X(I),Y(I),V1(I),V2(I))
      IJ=IJ+3
  100   CONTINUE
      NP=NP+3
      RETURN
      END
```

```
      SUBROUTINE ROWFIL(A,X,Y,DX,DY,NP)
      DIMENSION A(NP)
      COMMON/DIPLS/MYE,NXE,X00,Y00,Z00
      COMMON /GRID/ NGD,XG(50),YG(50)
      CALL ZERO(A,NP)
C  PUT ORIGEN OF COORDINATES AT CENTER OF SOURCES
      IJ=1
      Z=0.0
      Z0=Z00
CY0=Y00
      FORPI=12.566371
      GAM=-(Z-Z0)
CDO 100 J=1,MYE-1
      DO100 IJ=1,NGD
      X0=XG(IJ)-DX/2.
      Y0=YG(IJ)-DY/2.
      S0=Y-Y0
      S1=S0-DY
CX0=X00
CDO 50 I=1,NXE-1
      E0=X-X0
      E1=E0-DX
      T11=GAM*GAM+S1*S1+E1*E1
      T10=GAM*GAM+S1*S1+E0*E0
      T01=GAM*GAM+S0*S0+E1*E1
      T00=GAM*GAM+S0*S0+E0*E0
      S11=SQRT(T11)
      S00=SQRT(T00)
      S10=SQRT(T10)
      S01=SQRT(T01)
      F1=(ATAN(E1*S1/(GAM*S11))-ATAN(E0*S1/(GAM*S10))
     A  -ATAN(E1*S0/(GAM*S01)) + ATAN(E0*S0/(GAM*S00)))/FORPI
      A(IJ)=F1
      GO TO 51
      CALL IGRATE(X,Y,Z,FUL,FUR,FLL,FLR,DX,DY,X0,Y0,Z0)
      A(IJ)=A(IJ)+FUL
      A(IJ+1)=A(IJ+1)+FUR
      A(IJ+NXE)=A(IJ+NXE)+FLL
      A(IJ+NXE+1)=A(IJ+NXE+1)+FLR
  51    CONTINUE
CIJ=IJ+1
CX0=X0+DX
   50   CONTINUE
C     IJ=IJ+1
CY0=Y0+DY
  100   CONTINUE
      RETURN
      END
```

```
      SUBROUTINE IGRATE(X,Y,Z,FUL,FUR,FLL,FLR,DX,DY,X0,Y0,Z0)
      DIMENSION ETA(2),SI(2),DUM(4),TN(4),D1(4),D2(4),T(4)
C  CALCULATES APPROXIMATE DIPOLE MOMENT FOR ELEMENTS FO THE
C  GRID
      S2=S1+DY
      E2=E1+DX
C     WRITE(4,1000) S0,E0,S1,E1
 1000 FORMAT(10G)
      T02=GAM*GAM+S0*S0+E2*E2
      T20=GAM*GAM+S2*S2+E0*E0
      T22=GAM*GAM+S2*S2+E2*E2
      T12=GAM*GAM+S1*S1+E2*E2
      T21=GAM*GAM+S2*S2+E1*E1
      S02=SQRT(T02)
      S20=SQRT(T20)
      S22=SQRT(T22)
      S12=SQRT(T12)
      S21=SQRT(T21)
      F2=(ATAN(E2*S1/(GAM*S12))-ATAN(E1*S1/(GAM*S11))
     A  -ATAN(E2*S0/(GAM*S02))+ATAN(E1*S0/(GAM*S01)))
     A  /(FORPI*DX)
      F3=(ATAN(E1*S2/(GAM*S21))-ATAN(E0*S2/(GAM*S02))
     A  -ATAN(E1*S1/(GAM*S11))+ATAN(E0*S1/(GAM*S01)))
     A  /(FORPI*DY)
      F4=(ATAN(E2*S2/(GAM*S22))-ATAN(E1*S2/(GAM*S21))
     A  -ATAN(E2*S1/(GAM*S12))+ATAN(E1*S1/(GAM*S11)))
     A  /(FORPI*DX*DY)
      FUL=F1-F2-F3+F4
      FUR=F2-F4
      FLL=F3-F4
      FLR=F4
      WRITE (4,1080) F1,F2,F3,F4
      WRITE(4,1080) FUL,FUR,FLL,FLR
 1080   FORMAT(10G)
      RETURN
      END
```

```
      SUBROUTINE PRNT(IDS,X,N)
      DIMENSION X(N)
      WRITE(IDS,1001) X
 1001   FORMAT(1H ,/,(1H ,10(1PE11.2)))
      RETURN
      END
```

```
      SUBROUTINE ZERO(A,N)
      DIMENSION A(N)
      DO 10 I=1,N
      A(I)=0.0
   10   CONTINUE
      RETURN
      END
```

```
      SUBROUTINE MULT(A,P,M,N,V)
      DIMENSION A(1),P(1),V(N)
C     WRITE(6,1016)
 1016   FORMAT(1H ,'VECTOR READ INTO MULT')
      J=1
      DO 7 I=1,M
      V(I)=PROD(A(J),P,N)
      J=J+N
  7     CONTINUE
      RETURN
      END
```

```
      FUNCTION PROD(X,V,N)
      DIMENSION X(1),V(1)
      PROD=0.0
      DO 6 K=1,N
      PROD=PROD+X(K)*V(K)
    6   CONTINUE
      RETURN
      END
```

```
C SUBROUTINE TO ADD RANDOM NOISE TO CALCULATED VOLTAGE VALUES

      SUBROUTINE ADNOIS(V,NOBS,SCALE)
      DIMENSION V(1)
      S2=SCALE/2.
      N=5
      DO 6 I1=1,NOBS
      RDM=RAN(N)
      VNOS=RDM*SCALE
      V(I1)=V(I1)+VNOS-S2
    6   CONTINUE
      RETURN
      END
```

```
C SUBROUTINE TO COPY ORIGINAL A MATRIX AND SAVE AS AM
      SUBROUTINE SWITCH(A,AM,NOBS,NP)
      DIMENSIONA(1),AM(1)
      N=NP*NOBS
      DO 10 I=1,N
      AM(I)=A(I)
   10   CONTINUE
      RETURN
      END
```

```
C SUBROUTINE TO PRINT AMATRIX
      SUBROUTINE PRNTM(IDS,A,NOBS,NP)
      DIMENSION A(1)
      J=1
      DO 8 I=1,NOBS
      CALL PRNT(IDS,A(J),NP)
      J=J+NP
    8   CONTINUE
      RETURN
      END
```

```
C CALCULATES THE PRODUCT OF THE TRANSPOE OF A MATRIX AND A VECT
      SUBROUTINE VSTR(A,V,NOBS,NP,VSTAR)
      DIMENSION A(1),V(1),VSTAR(NOBS)
C      WRITE(6,1234) NOBS,NP
 1234 FORMAT(' VSTR:',5I5)
      DO 11 I1=1,NP
      VSTAR(I1)=PROCT(A(I1),V,NOBS,NP)
C      WRITE(6,1000) VSTAR(I1)
 1000 FORMAT(' VSTAR=',G)
   11   CONTINUE
      RETURN
      END
```

```
C CALCULATES THE PRODUCT OF A COLUMN OF A MATRIX AND A VECTOR
      FUNCTION  PRDCT(U,V,M,N)
      DIMENSION U(1),V(1)
      J=1
      PRDCT=0.0
      DO 12  I=1,M
      PRDCT=PRDCT+V(I)*U(J)
      J=J+N
   12   CONTINUE
      RETURN
      END
```

```
C CALCULATES PSTAR  FROM SINGULAR VALUES AND VSTAR
      SUBROUTINE PSTR(D,S,VSTAR,PSTAR,NOBS)
      DIMENSION VSTAR(1),PSTAR(1),S(1)
      D2=D*D
      DO 13 I=1,NOBS
      DEN=S(I)*S(I)+D2
      PSTAR(I)=(S(I)*VSTAR(I))/DEN
   13   CONTINUE
      RETURN
      END
```

```
C FUNCTION TO NEGLECT EIGEN VECTORS WHICH WHICH ARE 0
      FUNCTION NEIG(S,NP)
      DIMENSION S(NP)
      TEST=1.E-07*S(1)
      NEIG=1
      DO 21 I=2,NP
      IF(S(I).LT.TEST) GO TO 22
      NEIG=I
   21   CONTINUE
   22   RETURN
      END
```

```
C SUBROUTINE TO CALCULATE ERROR BETWEEN VNEW AND V
      FUNCTION ER1(VN,V,NOBS)
      DIMENSION VN(1),V(1)
      S=0.0
      DO 25 I=1,NOBS
      D1=VN(I)-V(I)
      DD=D1*D1
      S=S+DD
   25   CONTINUE
      ER1=SQRT(S/FLOAT(NOBS))
      RETURN
      END
```

```
      SUBROUTINE FOLSOR(A,V,X,Y,V1,V2)
      DIMENSION A(4)
C
C       FOR BIPOLE-MONOPOLE SOURCE FOLLOW SIMULATION
C
C       SOURCE ELECTRODE POSITIONS:
C       SOURCE 1 AT 0,0 AND XS1,YS1
C       SOURCE 2 AT 0,0 AND XS2,YS2
C
C       X21,Y21,X22,Y22 ARE THE SQUARES OF XS1,YS1,XS2,YS2
C
C       SOURCE1 GIVES V1+C1 AT X,Y
C       SOURCE2 GIVES V2+C2 AT X,Y
C       UNIT SOURCE POINTING AT X,Y GIVES V AT X,Y
C
C       A(1) MULTIPLIES UNKNOWN C1
C       A(2) MULTIPLIES UNKNOWN C2
C       A(3) MULTIPLIES UNKNOWN RESISTIVITY 1
C       A(4) MULTIPLIES UNKNOWN RESISTIVITY 2
C
      COMMON /SOURC/ XS1,YS1,XS2,YS2,X21,Y21,X22,Y22
      X2=X*X
      Y2=Y*Y
      COSA=(XS1*X+YS1*Y)/SQRT((X21+Y21)*(X2+Y2))
      COSB=(XS2*X+YS2*Y)/SQRT((X22+Y22)*(X2+Y2))
C     DENOM=SQRT(X21+Y21)*COSA + SQRT(X22+Y22)*COSB
C     DENOM=1.
      RI=1./SQRT(X2+Y2)
      TWPI=6.2832
C     CA=COSA/DENOM
C     CB=COSB/DENOM
      V=V1*COSA + V2*COSB
      A(1)=-COSA
      A(1)=A(1)/RI
      A(2)=-COSB
      A(2)=A(2)/RI
      A(3)=-COSA*(1./SQRT((X-XS1)**2+(Y-YS1)**2) - RI)/TWPI
     A     -COSB*(1./SQRT((X-XS2)**2+(Y-YS2)**2) - RI)/TWPI
      A(3)=A(3)/RI
C     A(1)=A(1)/A(3)
C      V=V/A(3)
C     A(2)=A(2)/A(3)
C     A(3)=A(3)/A(3)
      RETURN
      END
```

BIBLIOGRAPHY

Alpin, L. M., 1966, The theory of dipole sounding, in dipole methods for measuring earth conductivity: Consult. Bureau, New York, p. 1-60

Barakat, Richard; Blackman, Elliot; 1973, Application of the Tichonov Regularization Algorithm to Object Restoration: Optics Communications. v.9, No. 3, p. 252-256.

Businger and Golub, 1969, Algorithm 358=singular value decomposition of a complex matrix, Comm. ACM, v.12, no. 10, p.564-565

Dean, William C., 1958, Frequency Analysis for Gravity and Magnetic Interpretation: Geophysics, v.23, No. 1 p. 97-127.

Dey, Abhijit, Morrison, H. F., 1977, An Analysis of the Bipole-Dipole Method of Resistivity Surveying: Geothermics, v.6, p. 47-81.

Furgerson, Robert B., Keller, George V., 1974, Computed dipole resistivity effects for an earth model with vertical and lateral contrasts in resistivity: Off. Naval Res. Rep. of Investigations, Colorado School of Mines.

Golub, G. H., Reinsch, C., Singular Value Decomposition and Least Squares Solutions, 1970, Numer. Math, v.14, p. 403=420.

Hewlett-Packard, 1976, HP-67, Programmable Pocket Calculator, (intrinsic statistical functions).

Keller, George V., Frischknecht, Frank C., 1966, Electrical Methods in Geophysical Prospecting: Pergamon Press, Inc., Oxford.

Keller, George V., 1968, Electrical Prospecting for Oil: Colorado School of Mines Quarterly, v. 63, No. 2.

Keller, George V., Furgerson, R. B., Harthill, N., Jacobson, J. J., 1975, The dipole mapping method: Geophysics, v. 40, No. 3, p. 451-472.

Keller, George V., Theory of Quasi-Direct Location of Oil with Electrical Prospecting Methods. Unpublished.

McGreogor and Biggs, C. A., 1968, Belle Creek Montana: a rich stratigraphic trap: Amer. Assoc. Petrol. Geol. Bull., v. 52, no. 10, p. 1869-1877

Peters, Leo J., The direct approach to Magnectic interpretation and its application: Geophysics, v. 14, no. 3, p. 290-320

Roy, Amalendu, 1966, Downward continuation and its application to electromagnectic data interpretaion: Geophysics, v. 31, no. 1, p. 167-184

Stoyer, C. H., 1979, (personal communication)

Zohdy, Adel A. R., 1978, Total field resistivity mapping and sounding over horizontally layered media: Geophysics, v. 43, no. 4, p. 748-766